BEHAVIOR OF HIGH STRENGTH REINFORCED CONCRETE BEAMS WITH VARIOUS REINFORCEMENTS

A Thesis

Presented in Partial Fulfillment of the Requirements for the
Degree of Master of Science

with a

Major in Civil Engineering

in the

College of Graduate Studies

University of Idaho

by

Abdullah Almakrab

Major Professor: Ahmed Ibrahim, Ph.D.

Committee Members: S.J. Jung, Ph.D., Richard Nielsen, Ph.D.

Department Chair: Patricia J. S. Colberg, Ph.D.

December 2017

Authorization to Submit Thesis

This thesis of Abdullah Almakrab, submitted for the degree of Master of Science with a Major in Civil Engineering and titled "BEHAVIOR OF HIGH STRENGTH REINFORCED CONCRETE BEAMS WITH VARIOUS REINFORCEMENTS" has been reviewed in final form. Permission, as indicated by the signatures and dates below, is now granted to submit final copies to the College of Graduate Studies for approval.

Major Professor: _____ Date: _____
Ahmed Ibrahim, Ph.D.

Committee Members: _____ Date: _____
Richard Nielsen, Ph.D.

_____ Date: _____
S.J Jung, Ph.D.

Department Chair: _____ Date: _____
Patricia J. S. Colberg, Ph.D.

Abstract

The main goal of this study is to investigate the behavior of high strength concrete beams reinforced with various reinforcement under monotonic loading with various shear span-to-depth ratios and to compare the measured load-deflection history with the available prediction equations. In this study, eight high strength concrete (HSC) beams were prepared and cast using a concrete strength of 10 ksi. All beams spanned 7 ft. and were 12 inches deep and 6 inches' wide. Some of beams were reinforced with conventional #5 steel and others were reinforced with carbon fiber (CF) and glass fiber grids. Three beams were reinforced with #3 stirrups at 8 inches spacing and one beam was reinforced with #3 stirrups at 3-inch spacing. The beams were simply supported under monotonic four-point bending load using a servo-valve actuator with a capacity of 75 kips under three shear span-to-depth ratios. The data collected in this study included load-displacement-history at midspan, steel and carbon fiber strains, mode of failure and crack patterns. The experimental results were compared to analytical models from the literature. The models are very commonly used to predict the effective moment of inertia of reinforced concrete beams and consequently predict the deflection at the cracking and at the ultimate loads.

The study concluded that the behavior of the HSC beams was dependent on the type of reinforcement and on the shear span-to-depth ratio as well as the availability of transverse reinforcement. The analytical models, predictions of failure ultimate loads and mode of failure were in good agreement with the experimental results. For the HSC beams reinforced with steel bars, Branson's deflection equation highly overestimated the deflection. For beams reinforced with CFRP and GFRP grids, the analytical equations underestimated the

deflection at the midspan, which suggests the need to modify the existing deflection equations when HSC is reinforced with carbon fiber grids.

Keywords: Reinforced Concrete, High Strength, Carbon Fiber Grids, Deflection, Effective moment of Inertia

Acknowledgements

To my advisor, Dr. Ahmed Ibrahim, I am heartily grateful for the inspiration, encouragement, motivation and support he provided me throughout my thesis and graduate studies. Working with him was an opportunity of great learning experience. The patience he had for explaining concepts related to this research and in reading reports written by a non-native English speaker is greatly appreciated. Without his help and continuous support this work would not have been possible. My sincere and profound thanks are due to Dr. Richard Nielsen and Dr. S. Jung for serving as members of my thesis reviewing committee.

I would also like to thank Nick Saras and Moha Mudqiq for the help they provided during preparing and testing of the specimens. Also thanks to Don Parks for his technical support when needed. This work would not have been possible without their support as well. I would like to extend my thanks to Jesse Espy, the manager of Pre-Mix Inc. for his generous donation of the concrete mixtures needed to accomplish the work done in this thesis.

Acknowledgement is also due to the Department of Civil and Environmental Engineering at the University of Idaho for the support given to this research through its facilities and for granting me the opportunity to pursue my graduate studies with financial support. I would once again like to thank the University of Idaho for having such a great atmosphere on campus for International students.

Dedication

This work is dedicated to my father Saeed Almakrab, my mother Zahraa, and all my friends in Moscow, Idaho for their constant prayers, guidance, encouragement and invaluable support throughout my studies. Without their moral support, this would not have been possible.

Table of Contents

List of Tables

List of Figures

CHAPTER 1: INTRODUCTION

1.1 PROBLEM STATEMENT

The goal from the study is to investigate the behavior of high strength concrete beams reinforced with various reinforcement tested under shear span-to-depth ratios, and to validate the applicability of ACI deflection equations in predicting the deflection under service loads. To better understand the response of high-strength concrete beams failing in flexure and shear with and without shear reinforcement, eight reinforced concrete beams were tested under monotonic loads until failure. The beams were reinforced with various shear and carbon, and glass fiber grids. The concrete compressive strength of the tested beams was 69 MPa on average. The primary design variables were the amount and type of shear and longitudinal reinforcement. The load-displacement history of the tested beams was compared to the load-deflection equations in the literature and the results were compared. This study is part of a current project that is expected to test more beams under different parameters such as using hybrid reinforcement (steel bars and fiber reinforcement together). The study will be useful for researchers to report the behavior of HSC beams reinforced with fiber grids under various shear span-to-depth ratios and how applicable the existing ACI equations are to such beams. The test results are presented and discussed, and the influence of each design parameter is studied.

1.2 OBJECTIVE OF RESEARCH

The primary objective of this study is to investigate the shear and flexure behavior of high strength concrete beams reinforced with various reinforcement types, and under multiple shear-to-span depth ratios. The load-strain, load displacement, mode of failure, and midspan

deflection' histories were observed and compared with the current ACI design code to conduct a validity study. The second goal is to evaluate the HSC beams deflections using available empirical and code equations.

CHAPTER 2: LITERATURE REVIEW

2.1 INTRODUCTION

Many structures suffer from premature structural decay because of steel reinforcement corrosion. The physical evidence of this problem is certainly visible in the form of rust, major cracking and spalling concrete. The projected design life of conventional reinforced concrete structures is frequently shortened due to corrosion of the steel reinforcement. Some structures such as bridge decks are vulnerable to direct exposure of high concentrations of chlorides and deicers used for snow and ice removal. Typically, state departments of transportation (DOT) reinforcement cover and epoxy rebar specifications do not prevent the predictable penetration of deicers into the concrete. Extensive efforts have been reported in the literature to protect steel from corrosion, such as decreasing concrete permeability, reinforcing structures with epoxy-coated steel bars, increasing reinforcement cover requirements, and cathodic protection procedures. Typically, these methods are more successful at delaying the corrosion process than eliminating it. An alternative strategy to protecting the steel reinforcement is direct replacement of corrosion resistant steel. In this context, fiber-reinforced polymer (FRP) materials have significant potential. Corrosion resistant reinforcement steel (FRP materials) possess three important physical properties: (1) high tensile strength; (2) low elastic modulus; and (3) elastic-brittle stress-strain behavior.

To date, various studies have been published characterizing the behavior of FRP-reinforced concrete beams and slabs (Goodspeed et al. 1990; Brown and Bartholomew 1993; Banthia et al. 1995; Benmokrane et al. 1996; Bank et al. 1997; Masmoudi et al. 1998). However, strength and deflection prediction of steel-reinforced concrete beams is, in part, dependent on empirical performance constants. The empirical component reflects the

material specific composite behavior of steel and concrete. Therefore, where FRP is used in lieu of steel, the measured load-strain and load-displacement histories may well be altered beyond that predicted according to traditional concrete theory using simple substitution of reinforcement material properties such as the elastic modulus, the yield strength, and the failure strain. FRP grids are available in several geometric shapes including deformed circular bars and various 2D and 3D grids and cages. The FRP grid reinforcement used in this study is a rigid 2D grid commercially known as NEFMAC (NEFCOM Corp., Tokyo). More details about NEFMAC will be introduced later in Chapter 2.

In the following sections, a summary of the up-to-date literature on the behavior of concrete members reinforced with carbon fiber grids will be introduced and discussed.

2.2 HIGH STRENGTH CONCRETE

In 1984, the high strength concrete classification system was created by the American concrete institute (ACI) and define as the concrete mix with compressive strength greater than 6000 psi (41 MPa). However, The ACI found that this value might change depending on various factors such as the environments of concrete placement and location of structures site. For example, some areas have high temperature climates, which make the concrete dry quickly, which weakens compressive strength. Classification system was developed by Prof. J. Francis Young of the University of Illinois at Champaign-Urbana, (see Table 2.1).

Table 2.1: Concrete Strength Classifications

	Conventional concrete	High-strength concrete	Very-high-strength concrete	Ultra-high-strength concrete
Strength, MPa (psi)	< 50 (7250)	50-100 (7250-14,500)	100-150 (14,500-21,750)	> 150 (21,750)
Water-cement ratio	> 0.45	0.45-0.30	0.30-0.25	< 0.25
Chemical admixtures	Not necessary	WRA/HRWR*	HRWR*	HRWR*
Mineral admixtures	Not necessary	Fly ash	Silica fume**	Silica fume**
Permeability coefficient (cm/s)	$> 10^{-10}$	10^{-11}	10^{-12}	$< 10^{-13}$
Freeze-thaw protection	Needs air entrainment	Needs air entrainment	Needs air entrainment	No freezable water

* WRA = Water reducing admixture; HRWR = high-range water reducer
** Also may contain fly ash

2.3 CFRP GRIDS: NEFMAC

NEFMAC is the commercial name of 2D FRP grid that was used in this study. (‘‘New’’ 1988; ‘‘Mechanical’’ 1990). NEFMAC produced using pin-winding process that involves layering separate fiber-resin laminations, (Yost et al. 2001). NEFMAC has a volume of fiber about 40% (Yost el al. 2001). Figure 2.1 shows a typical 2D FRP grid.

In Yost and Schmeckpeper (2001) study of concrete bridge deck specimens reinforced by various NEFMAC grids, seven specimens were prepared; three were reinforced with H22 NEFMAC and three reinforced with C22 NEFMAC and a single control slab were prepared. The H22 is the hybrid glass-fiber and C22 is only carbon grids (Yost et al. 2001). The samples had a typical depth of 216 mm (8.5 in.) and span 2.44 m (8 ft.). All NEFMAC samples were reinforced with 11 longitudinal bars equally spaced at 100 mm (4 in.). The control steel sample was reinforced with 11 No. 5 Grade 60 bars equally spaced at 112 mm (4.4 in.). The authors monitored the strain behavior of the samples using conventional strain gages, where the gages were mounted on the FRP grid and on the concrete surface. Deflection was measured using linear variable deflection transducers. All slabs were tested under a constant shear span to depth ratio of 5.5 and the loads applied were

monotonic and cyclic loads. The study concluded that the results showed low working stress levels in the reinforcement and a high degree of reserve strength and a greater cross-sectional area of the NEFMAC grid, compared to steel reinforcements is required (Yost and Schmeckpeper 2001).

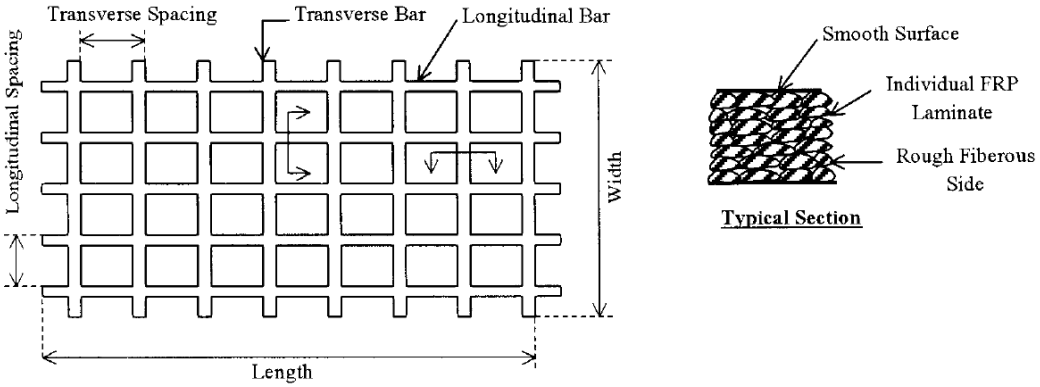

Figure 2.1: Typical NEFMAC 2D Grid (Yost et al. 2001).

Yost et al. (2001) investigated the flexural behavior of simply supported concrete beams reinforced with FRP grids under four-point monotonic loading as shown in Figure 2.2. The key parameter studied were the percentages of longitudinal FRP reinforcement. The beams were divided into three groups; balanced strain condition, under-reinforced and over-reinforced sections. The experimental results included load-deflection, failure mode, and cracking behavior. The strain in the reinforcing steel were compared with theoretical predictions calculated per conventional steel-reinforced concrete procedures (ACI 318-16).

It was concluded the flexural capacity was accurately predicted, but shear strength was not. It was observed that flexural stiffness was less than that predicted by Branson's equation. The moment-curvature relationship was in good agreement with the experimental results. The developed moment-curvature relationship was based on a bilinear (stress-strain

relationship) concrete model. It was also noticed that the fiber grid produced a transverse force path throughout the tested beams (Yost et al. 2001). It was concluded that:

- The flexural capacity of NEFMAC reinforced concrete beams could be accurately predicted using ACI 318.
- The shear capacity of NEFMAC-reinforced beams was overestimated by ACI 318, based on the premature shear failure of under reinforced samples.
- The authors (Yost el al. 2001) also concluded that there was an inverse correlation between the magnitude of stiffness overestimation and the amount of longitudinal NEFMAC reinforcement.
- The authors calculated the reinforcement strain using a bilinear concrete model and linear strain distribution, which was very accurate.
- The authors recommended the flexural design of FRP-reinforced concrete beams most likely requires over reinforcement to compensate for deflection tolerances and the reinforcement's elastic-brittle failure characteristic.

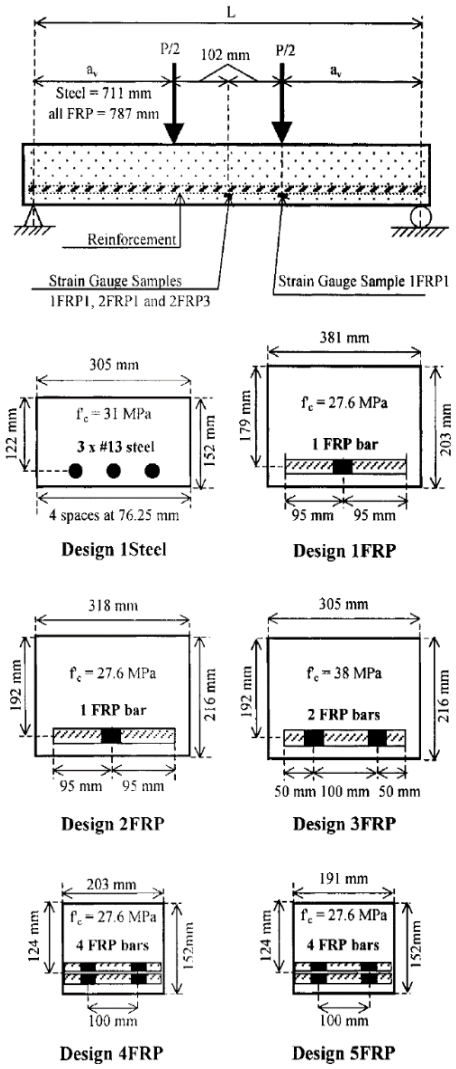

Figure 2.2: Test Setup and Sample Details (Yost et al. 2001).

Yang et al. (2017) investigated the damage behavior of concrete beams reinforced with glass fiber reinforced polymer (GFRP). The study was performed using finite element modeling using ABAQUS with a full consideration of materials nonlinearity. The finite element output was compared to experimental results with key parameters included such as the effect of replacing steel reinforcement by different types of GFRP bars. The study showed that the hybrid effect of reinforcement improved beam ductility and eliminated the unfavorable brittle failure of the concrete beam. In addition, it was suggested to use conventional compression steel bars in concrete beams with hybrid reinforcement. The study

also showed that in hybrid reinforced beams, a significant reduction in stiffness and a noticeable increase in the beams' deflection after the initiation of first crack and yielding of steel reinforcement were observed. On the counter part, in hybrid fiber/steel reinforced concrete beams showed a better performance during cracking initiation and propagation.

Yang et al. (2017) reported that the cracking of GFRP beams was relatively small and the maximum crack width, fractal dimension and deflections corresponding to the ultimate loads were relatively large compared with the typical results for steel-reinforced concrete beams. The finite element modeling accurately assessed the damage evaluation of the tested beams at all loading stages. The energy dissipation of conventional steel and GFRP were in very good agreement. However, GFRP and steel reinforcement bars exert clearly different influences on the plastic dissipation energy and strain energy of concrete beams, as demonstrated by the FE model as shown in Figure 2.3. Yang et al. 2015, defined the plastic energy as the energy related to the residual deformation the member experience. The plastic defamation is related to the type of loading and the rate where the load is applied.

Mustafa et al. (2017), reported the behavior of concrete beams reinforced with hybrid steel and FRP composites. The study was conducted using the nonlinear finite element code ANSYS. The parameters were the types of CFRP and GFRP bars in addition to conventional steel bars. The simulation was verified comparing the results with experimental work published in the literature. Figure 2.4 shows the good agreement between the experiments and the modeled beams in terms of cracking profile and yielding. The hybrid effect increased the ductility of the modeled beams and the higher the percentage of GFRP, the lower the rate of increase in the ultimate capacity and the lower the strength.

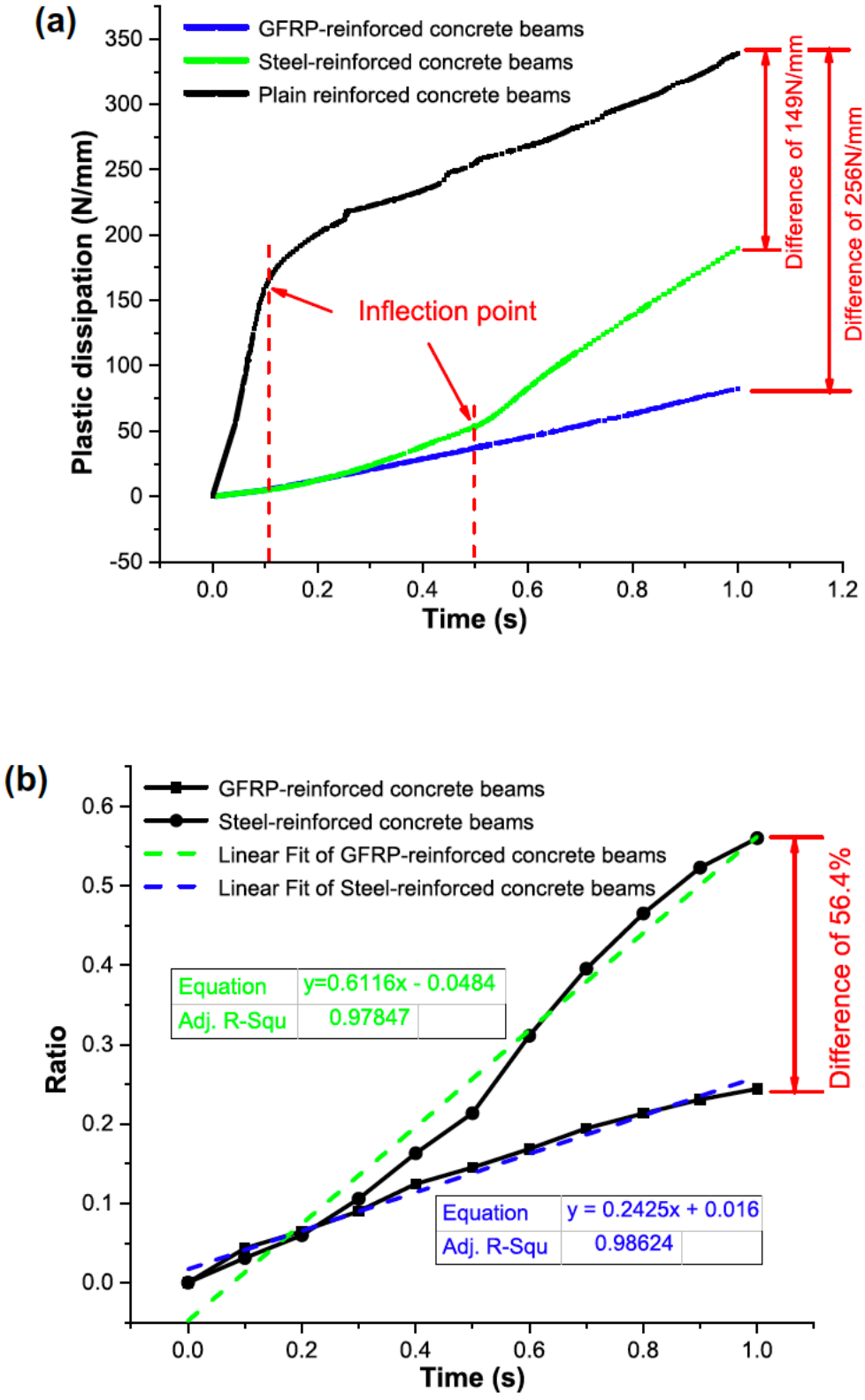

Figure 2.3: Plastic dissipation energy: (a) plastic dissipation energy values and (b) Plastic dissipation energy ratio.

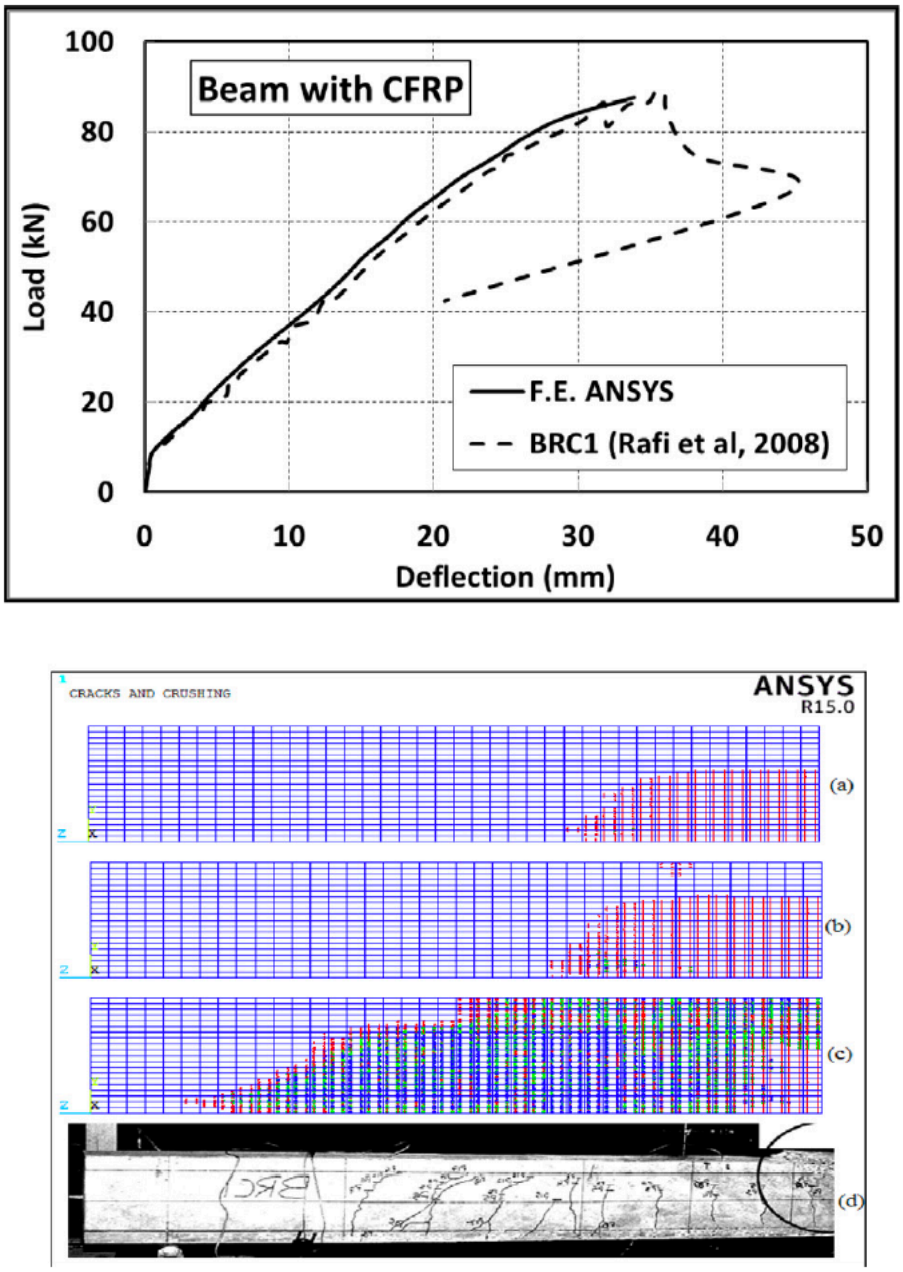

Figure 2.4: Comparison between the tested beam and the finite element results (Mustafa et al. (2017).

Goldston et al. (2017) experimentally investigated the flexural behavior of high strength concrete (HSC) and ultra-high strength concrete (UHSC) beams reinforced with glass fiber reinforced polymer (GFRP) bars. The compressive strength of HSC and UHSC were 80 and

120 MPa (11 ksi and 17.4 ksi), respectively. Beams of 2400 mm long, 100 mm wide and 150 mm high were tested under three-point loading. Three different bar GFRP sizes were used; #2, #3 and #4. The longitudinal GFRP tensile reinforcement ratios were 0.5%, 1.0% and 2.0% where all beams were reinforced in the tension and compression zones with GFRP bars. The influence of reinforcement ratio and compressive strength of high strength concrete (HSC) and ultra-high strength concrete (UHSC) on the load carrying capacity, deflection, energy absorption, strains in the concrete and reinforcement, and failure modes were investigated. The authors conducted materials testing to determine the GFRP properties in tension. Figure 2.5 shows the stress-strain behavior of the tested specimens with different diameters where explains the linear behavior of such glass fibers.

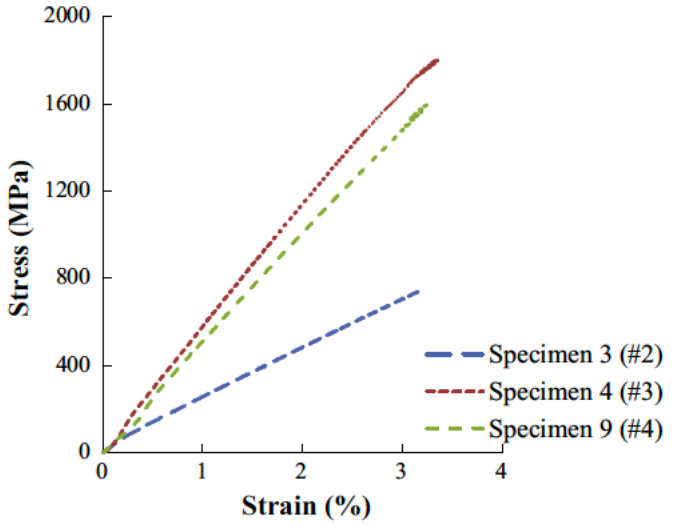

Figure 2.5: Stress-strain curve of GFRP tensile test specimens (Goldston et al. 2017).

Goldston et al. (2017) reported that the failure behavior of under-reinforced high strength and ultrahigh strength concrete glass fiber reinforced beams was ductile. Figure 2.6 shows the load-strain history for all beams. It can be seen that a drop-in strain when the section started to crack. The post-cracking behavior was function of the percentage of glass

fiber reinforcement. The strain in the glass fiber bars did not change with the change in concrete compressive strength, and it was noted that the strain in the ultra-high strength concrete was lower than the strain values in same beams made with high strength concrete at the same load level. More details could be found in Goldston et. al. (2017).

As expected, the energy absorbed by the ultra-high strength concrete was higher than the energy absorbed by the high strength concrete as shown in Fig. 2.6. Goldston et. Al. (2017) concluded that the flexural strength of fiber-reinforced polymer was found to be conservative, and un-conservative in the deflection calculations.

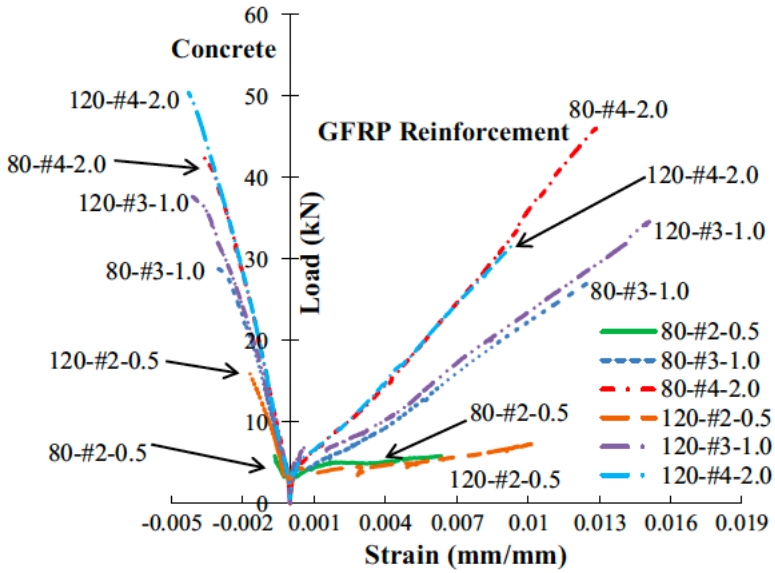

Figure 2.6: Load-strain behavior of GFRP-RC beams under static loading. (Goldston et. al), 2017).

Fang et al. (2017) investigated the mechanical performance of concrete pavement reinforced by CFRP grids for bridge deck application. This study is considered one of the few studies that investigated the structural performance of concrete reinforced by CFRP grids. The concrete pavement in the deck is steel fiber reinforced concrete (SFRC)

reinforced by CFRP grids. The study included experimental, analytical, and finite element investigations, where the slabs were tested under four-point bending at different locations of CFRP grids in the depth direction. The slabs were tested under positive and negative bending moments. Figure 2.7 shows a cross section of the tested slabs showing all the elements implemented in the study.

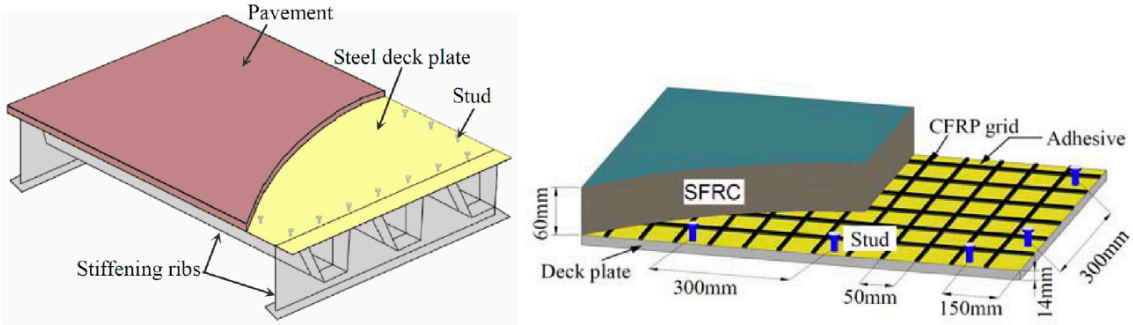

Figure 2.7: Illustration of a CPCG deck specimen (a) Pavement on an orthotropic steel bridge deck and (b) CPCG deck specimen with different components (Fang et al. 2017).

It was found that the CFRP grid improved the ultimate capacity of the deck by 60.22%, reducing the risk of the steel slab cracking under positive moment. The CFRP grid also reduced the ductility of the slabs under the negative moments.

This study compliments other experimental programs where FRP grid are investigated for similar applications (Bank et al. 1997 and Yost et al. 2002). NEFMAC grids have been implemented in concrete bridge decks and investigated by Benmokrane et al. (1999) to comprehend on the flexural design of concrete decks with such fiber reinforced polymer grids. The study also has included field monitoring of the NEFMAC being used as a major bridge deck reinforcement in (Joffre Bridge (located in Sherbrooke, Que., Canada).

Various other studies have been conducted on concrete members reinforced with fiber reinforced polymers (FRP grids). Rizkalla et al. (2012) introduced numerous developments in the implementation of the CFRP grids as reinforcement for precast concrete members.

Other researchers (Fang et al. 2004) have been studied the behavior of concrete slabs reinforced with carbon fiber grids. Fang et al. (2004) recommended that sections with fiber grids should be designed as over reinforced sections with an equivalent stiffness corresponding to steel reinforcement. The fiber carbon grids might be a good reinforcing tool to decrease the probability of shrinkage cracking to happen (Shao et al. 2007). Matthys et al. (2000) reported that the behavior of concrete members reinforced with carbon fiber grids are different that the conventional concrete beams reinforced with regular steel. The fiber grids have an additional property where it can transfer loading the transverse direction, which provides mechanical interlocking with concrete, (Engel et al. 1999). Other recommendation of using carbon fiber grids in bridge superstructures have been reported by Matta et al. (2005). The carbon fiber grids could be used in retrofitting in masonry walls as well as reported by Yost and Schmeckpeper (2001). Finally, Bank et al. (1997) demonstrated the usage of fiber grids on steel-concrete highway bridges.

2.4 DEFLECTION OF STRENGTH CONCRETE BEAMS

The utilization of high strength materials reinforcing together with high strength concrete makes it possible to design shallower flexural members, thus increasing the importance of estimating the deflections to satisfy serviceability limits of the codes (ACI 318-16). The term serviceability usually refers to control of deflections and crack widths at service loads for flexural members. Deflections of reinforced concrete flexural members were the focus of

various research for many decades and, (Sherif et al. 1998) thus, different methods have been proposed for deflection prediction under both short-and long-term loadings. The main factors affecting the short-term deflections of a beam are the span length, type and magnitude of loading, material properties, sectional dimensions and extent of cracks (Al-Zaid et al. 1991).

In 1965, Branson developed a well-known equation for the average effective moment of inertia over the entire length of a simply supported beam, subjected to uniform load. The ACI building code adopted this equation since 1971. The effect of loading types was not considered in this equation up to date. Various researchers developed equations for normal and high strength concrete deflection prediction. Rangan et al. (1982) developed a simple expression for controlling the deflection as a function of the span-depth ratio into account. Al-Zaid et al (1991) modified Branson equation to include the effect of loading type by considering the variations in the cracked length for each type of loading. Alsayed et al. (1993) presented an experimental model for predicting the deflection of fiber reinforced concrete beams.

In the next chapter, the experimental testing setup, the discussion of the results and the conclusions will be presented.

CHAPTER 3: EXPERIMENTAL PROGRAM

This chapter describes the testing setup, sample details, and the testing procedures.

3.1 MECHANICAL PROPERTIES OF HIGH STRENGTH CONCRETE (HSC)

Eight high strength concrete (HSC) reinforced beams were prepared and cast at the structural testing laboratory at the University of Idaho. The concrete was provided by the Pre-Mix Inc. located in Pullman, Washington. The target strength was 10 ksi with a slump value of 3 in. and maximum aggregate size of ¾ inch. All the concrete ingredients are shown in Table 3.1.

Three concrete cylinders 4 x 8 inches for the compressive strength test, one cylinder 6 x 12 in for the split tensile strength test and one beam (6 x 6 x 21 in.) for the flexural strength test were prepared from the batch. The compressive strength, split tensile strength and the flexural strength tests were performed per the ASTM standards C39, C496, and C78, respectively. According to ASTM C39, the average compressive strength of three specimens was 10 ksi, and the average split tension strength was 0.65 ksi. Figure 3.1 shows the compressive strength test.

Table 3.1 HSC Concrete mix proportions

Material	Batched Quantity	Moisture (%)	Actual Water (gl.)
3/4" CUBED	3020 lb.	0.10% M	-
BLEND SAND	2640 Ib.	4.07% A	12 gl.
TYPE I-II	1490.0 Ib.	-	-
DARAVAIR (AIR ENTRAIN.)	5.00 Oz	-	-
DARACEH (Con. SUPERPLASTICISER)	57.00 Oz	-	-
WATER	45.0 gl.	-	-
WATER/CEMENT RATIO	0.323	-	-

Figure 3.1: Compressive strength test

3.2 MECHANICAL PROPERTIES OF CARBON AND GLASS FIBER GRIDS

The 2D FRP grid used to reinforce the HSC beams is called NEFMAC and is manufactured by Toray Industries of Tokyo (NEFCOM 1988; NEFCOM 1990). NEFMAC grid consists of carbon fibers saturated in a vinyl resin with a rough fiber volume of 40%. For example, glass carbon fiber grid has 5% carbon fiber, 39% glass fiber, and 56% resin by volume (Schmeckpeper 1992; Yost et al. 2001). The fibers either pure carbon or hybrid (carbon and

glass) are manufactured to form a 2D rectangular orthogonal grid with symmetrical mechanical properties as shown in Figure 3.2, (Yost et al. 2001).

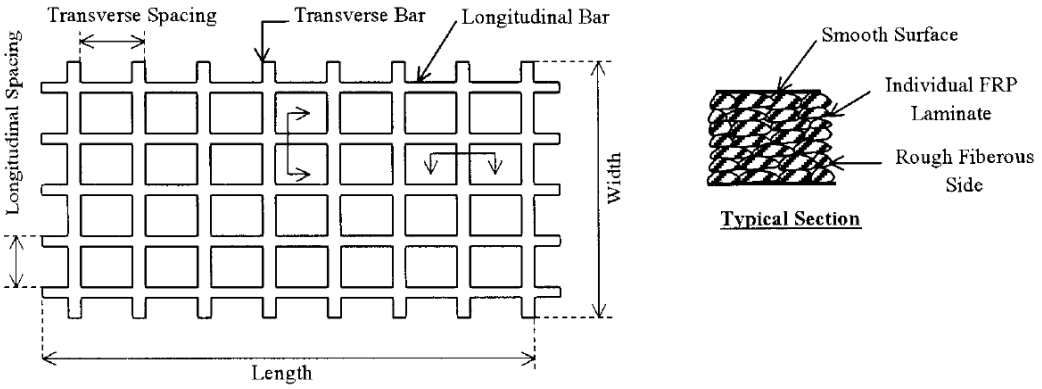

Figure 3.2: Fiber reinforced polymer grid (Schmeckpeper et al. 2001).

Bar identification as ‘‘longitudinal’’ or ‘‘transverse’’ is a function of orientation with respect to bending. Longitudinal and transverse bars provide tensile reinforcement and force transfer, respectively. The carbon fiber grid has a cross-sectional area of 80 mm^2 (0.124 in^2). The mechanical properties considered were the tensile strength, and elastic modulus. All mechanical properties are shown in table 3.2. The submerged volumetric method was used to determine the cross-sectional area while, and the mechanical properties were determined from uniaxial tensile tests conducted on full cross section bar samples (Schmeckpeper 1992).

The fiber grid bars used in this study are identified as CFRP and GFRP. The CFRP grid is a mixture of glass and carbon fibers and the GFRP grid is composed of glass fibers. Typical fiber materials has linear-elastic stress-strain behavior up to ultimate load at which brittle tensile failure usually arises as shown in Figure 3.3. Figure 3.4 shows the CFRP and the GFRP grids used to reinforce the beams in this study.

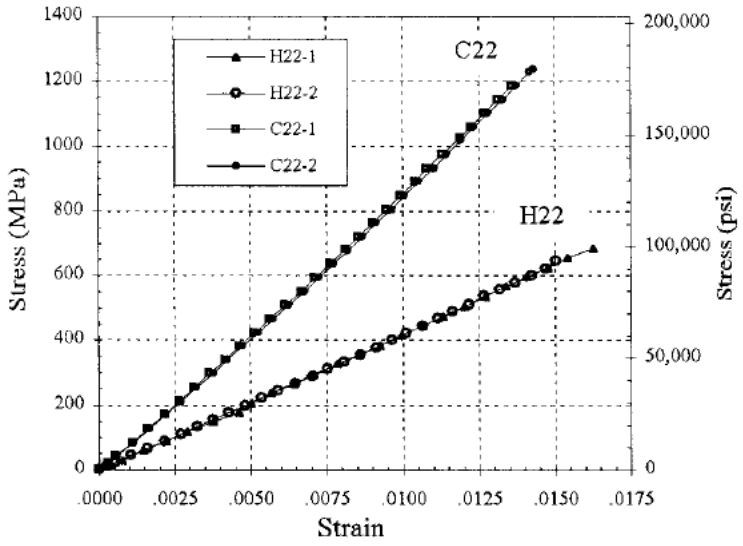

Figure 3.3: Fiber reinforced polymer grid (Yost et al. 2001).

Table 3.2 Properties of NEFMAC

Grid	**Carbon content (10%)**	**Glass fiber (10%)**	**Resin (%)**	**Depth (mm)**	**Width (mm)**	**Area (mm^2)**	***f_u (MPa)***	**E *(MPa)***
CFRP	36	0	64	21.25	21.25	451.61	1230	85000
GFRP	5	39	56	9	9	81	635	41300

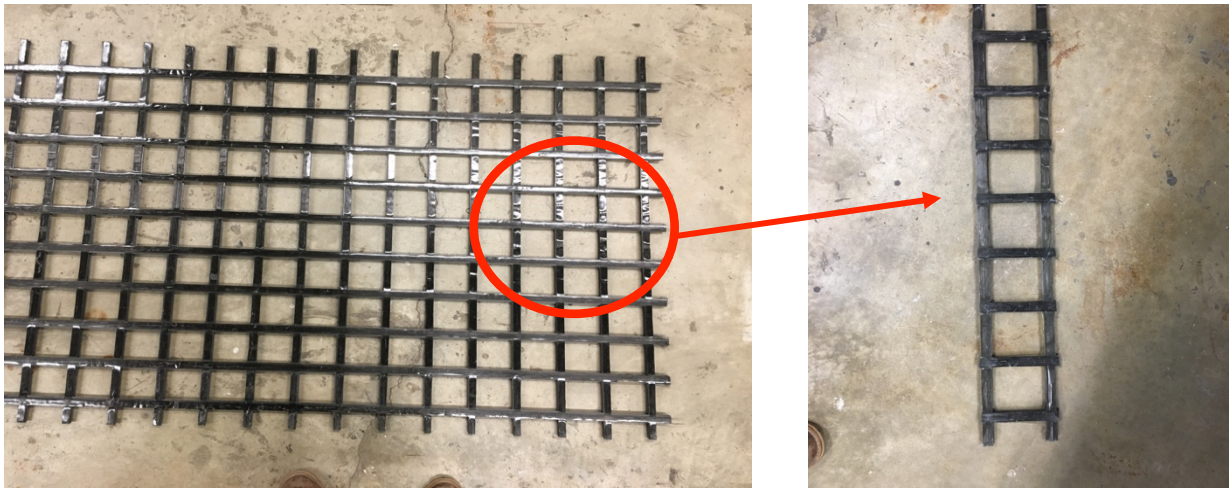

Figure 3.4a: CFRP grid

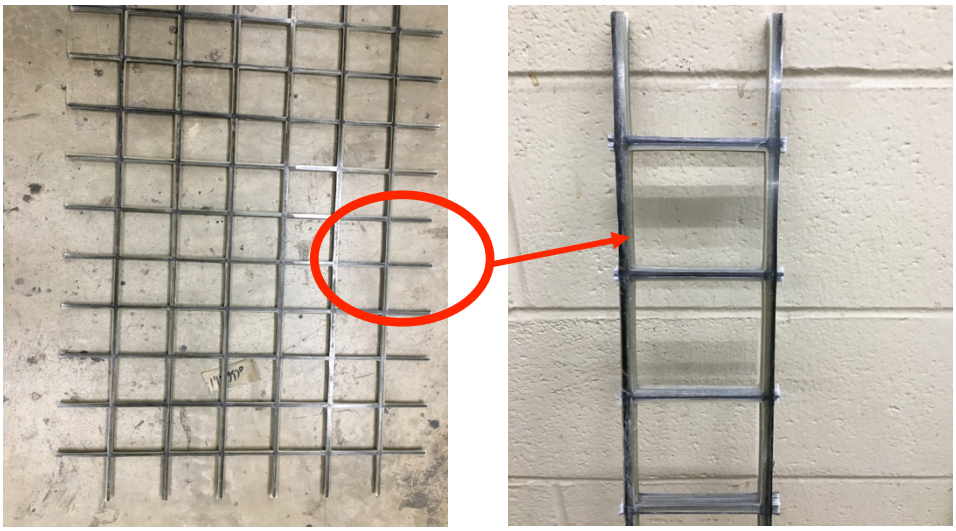

Figure 3.4b: GFRP grid

3.3 BEAM DETAILS

Testing was intended to evaluate flexural/shear behavior of high strength concrete beams strengthened with CFRP and GFRP grids. Eight beams were designed according the ACI 318-16 and tested under monotonic loading using a four-point bending test. The eight beams

were divided into three groups; the first group consisted of three beams having the same conventional flexural reinforcement steel, but different shear span-to-depth ratios without shear reinforcement. The second group consisted of three beams reinforced with same flexural reinforcement of group one shear reinforcement (stirrups) at different spacings and tested under different shear span-to-depth ratios. The third group was reinforced with the CFRP and GFRP grids without shear reinforcements.

The beams abbreviations were named as follows: Beam Number-Reinforcement-Loading-Type-Stirrups-Spacing-shear span. For example, 2CONT-MN-2 means beam number 2 as a control specimen (CONT)-monotonic loading (M) with no stirrups (N) and with a shear span of 2 feet. 8 CF-M8-2.5 stands for beam number 8 reinforced with carbon fiber (CF) under monotonic loading with 8-inch stirrup spacing and a shear span of 2.5. All beams have a total span of 7 feet and a clear span of 6.16 feet, and were tested as simply supported. The tension concrete cover was 1 inch and all the top and side covers were 0.50 inches. After 24 hours of casting, all forms were removed and all beams were covered with wet towels and cured for 28-days after they were kept at room temperature until the day of testing. Table 3.3 shows all beams' dimensions with all the reinforcement details. Figure 3.5 shows the formwork and the reinforcement cages of one of the tested beams, and Figure 3.6 shows all beams after casting. The cross sections of the tested beam are shown in Fig. 3.7 with all reinforcement details.

Figure 3.5: Beam 4 CONT-M8-2 formwork and reinforcement cage (left), and 8CF-M8-2.5 (right)

Figure 3.6: Beams after casting

Table 3.3 Beams Reinforcement Details

Beams	Group no.	Length (ft.)	Clear Span (ft.)	b (in.)	d (in.)	a (in.)	Bottom Reinforcement	Stirrups
2Cont-MN-2.5	1	7	6.16	6	11	2.5	2#5 Steel bar	None
3Cont-MN-2		7	6.16	6	11	3	2#5 Steel bar	None
4Cont-M8-2	2	7	6.16	6	11	2	2#5Steel bar	#3 @ 8"
5Cont-M8-2.5		7	6.16	6	11	2.5	2#5 Steel bar	#3 @ 8"
6Cont-M8-3		7	6.16	6	11	3	2#5 Steel bar	#3 @ 8"
7Cont-M3-2.5	3	7	6.16	6	11	2.5	2#5 Steel bar	#3 @ 3"
8CF-MN-2.5	4	7	6.16	6	11	2.5	CFRP grid	None
10GF-MN-2.5		7	6.16	6	11	2.5	GFRP grid	None

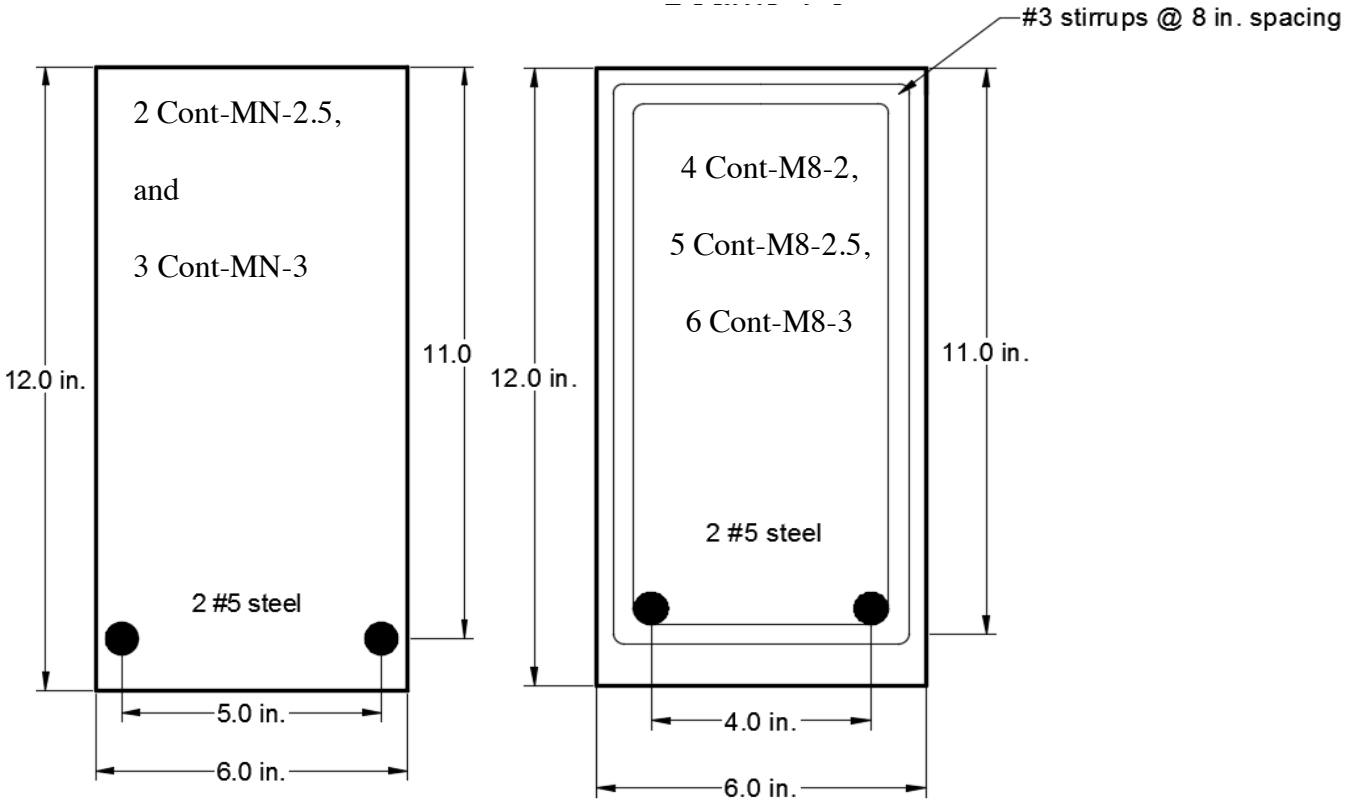
2 Cont-MN-2.5,
and
3 Cont-MN-3
12.0 in.
11.0
2 #5 steel
5.0 in.
6.0 in.
#3 stirrups @ 8 in. spacing
4 Cont-M8-2,
5 Cont-M8-2.5,
6 Cont-M8-3
12.0 in.
11.0 in.
2 #5 steel
4.0 in.
6.0 in.

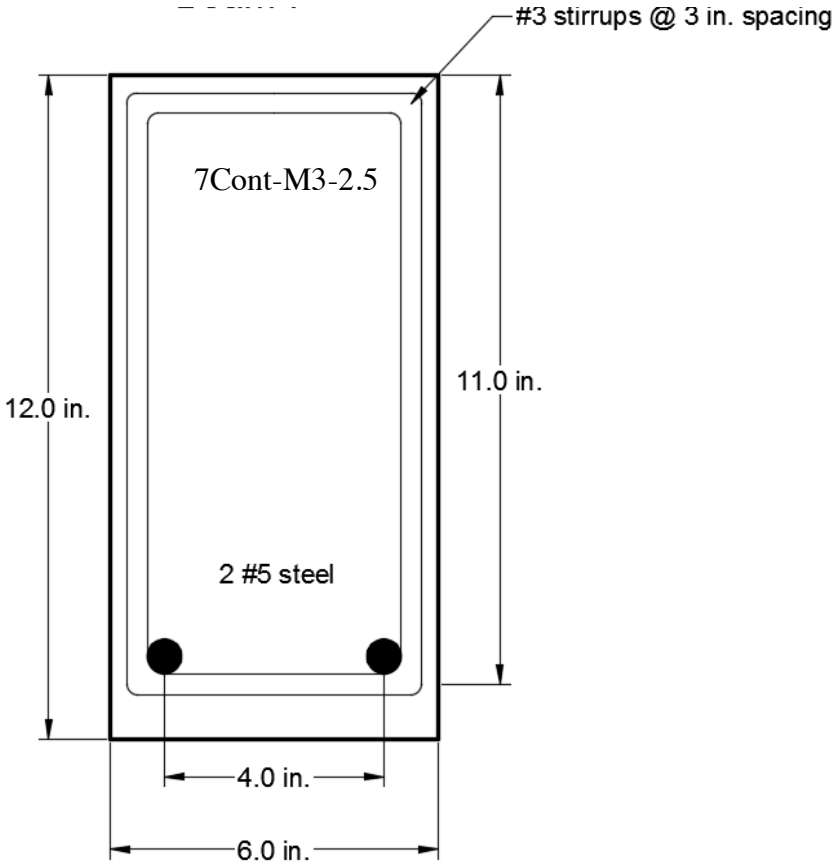
#3 stirrups @ 3 in. spacing
7Cont-M3-2.5
12.0 in.
11.0 in.
2 #5 steel
4.0 in.
6.0 in.

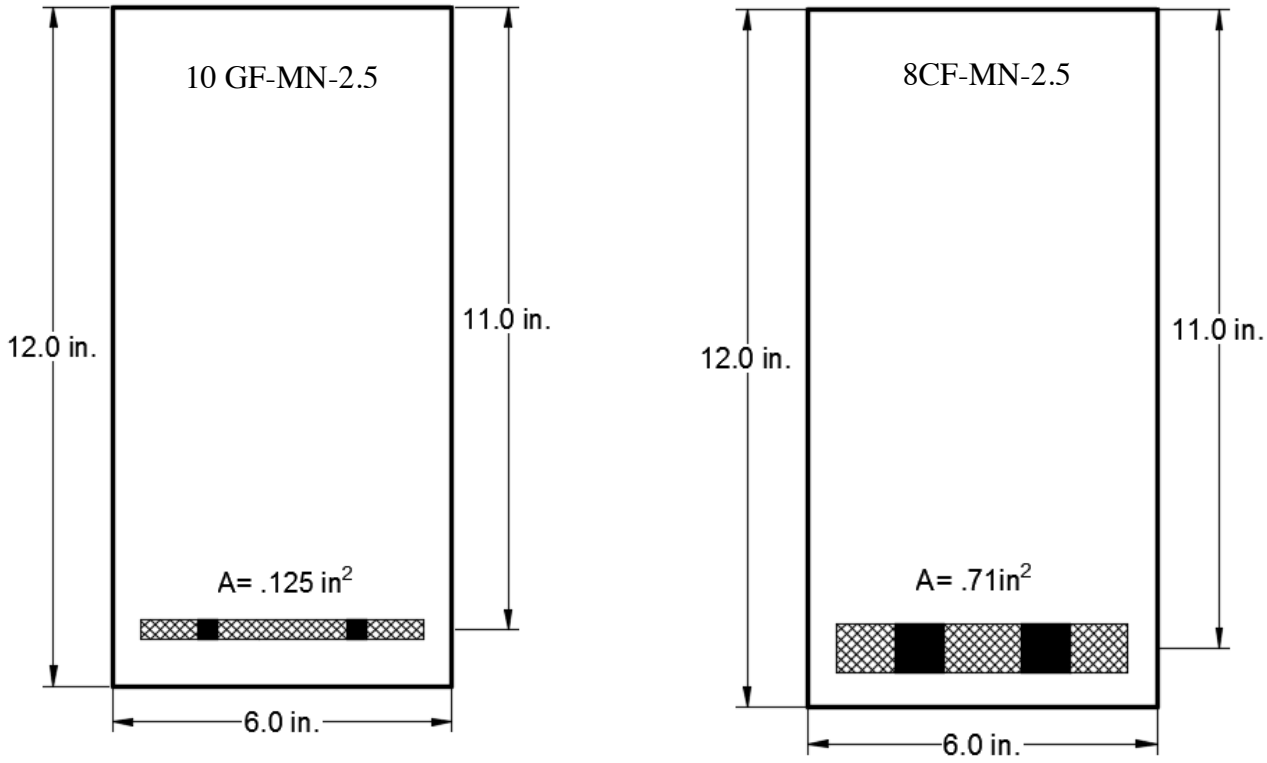

Figure 3.7: Beams cross sections with reinforcement details

3.4 BEAM TESTING SETUP

All beams were considered simply supported under four-point loading (Fig. 3.8). Span of all beams were 7 ft. (2133.6 mm), with a variable shear span and overhang of 0.5 ft. (152.4) mm on each side. One support was considered a hinge and the other support was considered a roller and the load was applied monotonically. A 220 kN servo-valve hydraulic actuator was anchored to a closed-loop steel frame, and the load was applied to the HSC beams through a steel spreader beam placed on the top of the concrete beam at the mid-span. All beams were tested under displacement controlled loading at the rate of 1 mm/min until failure or steel yielding, which happens first. Two strain gages were attached at the bottom two flexural reinforcement bars at the mid span, or in some other cases they were attached to

the first stirrup close to the beam ends (Fig. 3.9). An LVDT was positioned at the mid span of the beam to measure the deflection-time history. Cracks were marked and the corresponding loads were recorded during all beams testing. Data including load, mid-span deflection and strain were recorded using a high-speed data acquisition system

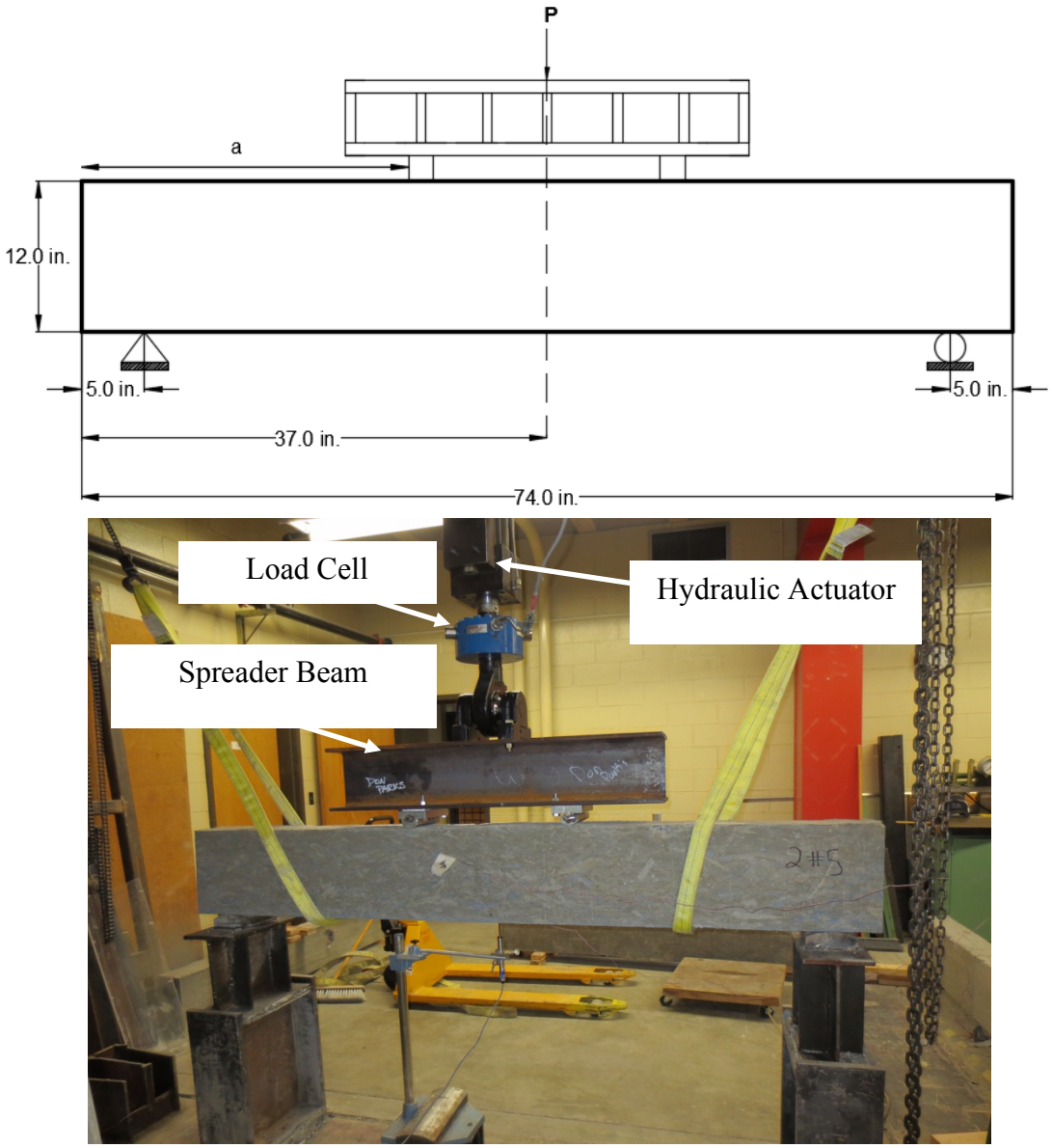

Figure 3.8: Schematic shows beams setup (a), and actual beam setup

3.4.1 Data Logger

A Delphin EL200 Expert Logger (32) Analog Input Channels Up to with a 1 kHz Sample Rate, 4/8 Digital Inputs/Outputs. USB and Ethernet 2Gb Internal Storage was used to collect the displacement of the beams. The data logger can process up to 46 analog input channels at both and high rates sampling rates (3 groups per 1000 Hz) with a resolution/input impedance of 24Bit/1GΩ. Figure 3.9 shows the data logger.

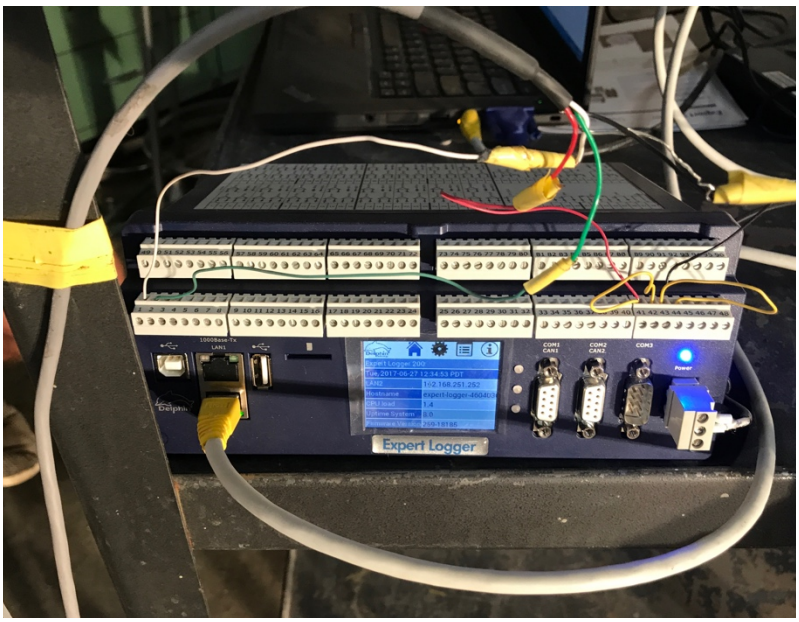

Figure 3.9: Expert logger 200

3.4.2 Strain Gages

Foil strain gages (CEA-06-125UN-350/P2, Vishay Inc.) were installed on tension bars to measure and investigate strains during beam testing, as shown in Figure 3.10. The surface of steel/fiber bars were cleaned with grinder without affecting the total cross-sectional area of the bars. The strain gages were glued to the bar surface using epoxy and then left 24-hous to

dry. The Self-fusing tape was used to protect the gages from moisture and other potential external distress. Strain conditioners were attached to all the gages to magnify the millivolt output of the gages and the gage factors for each gage was input to the data logger as specified by the manufacturer.

Figure 3.10: Strain gages installed at the bottom reinforcement.

3.4.3 Linear Variable Displacement Transducer

A linear displacement transducer (LVDT) was used and it has active 350-ohm strain-gage bridge to sense the movable rod displacement. The LVDT had a stroke range of 2 in (100 mm). Figure 3.11 shows the LVDTs used in this study.

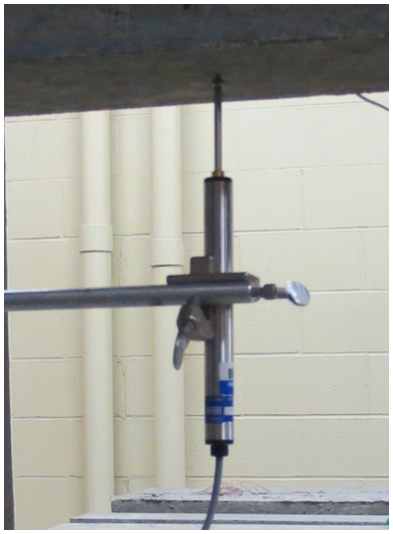

Figure 3.11: Strain gages installed at the bottom reinforcement

In Chapter 4, the results and discussion of eight HSC beams reinforced with conventional and fiber reinforcement grids will be discussed in details.

CHAPTER 4: RESULTS AND DISCUSSIONS

4.1 INTRODUCTION

In this chapter, the results and discussion of testing eight high strength concrete beams reinforced by conventional steel and fiber reinforced grids will be presented. The load displacement history and the strain in the main flexural and web steels are measured and presented. The results include the mode of failure; the load capacity, and the longitudinal steel/fiber strain profile. Special attention was paid to the selected parameters to gain a deeper understanding of the shear behavior and the fiber reinforced grid effect on the overall beam failure under monotonic loading. The beams were divided into three groups, the first group has no shear reinforcement and is reinforced on the tension side with 2#5 bars, the second group was reinforced with same main steel as group one with steel stirrups spaced at 8 inches, the third group was same as group two with stirrups spacing of 3 inches, and the final group were reinforced with CFRP and GFRP grids with no shear reinforcements. All beams had the same overall span length (7 ft.) and cross section of 6 x 12 inches as discussed in chapter 3.

4.2 TEST RESULTS

4.2.1 Group 1

The first group of beams had no shear reinforcement and was only reinforced with 2#5 longitudinal steel reinforcing bars. This group consisted of two beams and was tested under shear spans of 2.0 and 2.50. The concrete used in all beams were high strength concrete with a 28-day strength of 10 ksi. The test was stopped either when the concrete fails or the steel yields whichever reached first. Figures 4.1 and 4.2 show the failure mode of the two beams in group1 (3CONT-MN-2 and 2CONT-MN-2.5). The two beams failed under shear as

expected and the failure was sudden once the ultimate shear strength was reached. Flexural cracks started at the mid span at loads around 7.5 kips flexural cracks extended the depth of the beam until suddenly an inclined shear crack extended from one of the supports (left support as shown in Figure 4.1) to reach the top compression surface of the beam under the point load (shear span).

Figure 4.1: Beam 3CONT-MN-2 failure mode (shear failure).

Figure 4.2: Beam 2CONT-MN-2.5 failure mode (shear failure).

The load-strain relationship is also captured during testing as shown in Figure 4.4. Two strain gages were attached to the main bottom reinforcement's bar and the average strain was plotted as shown. As the load increases, tension strain in the bottom reinforcement increases with sudden failure of the beams has occurred. The bottom tensile strain of the two beams did not reach the yield strain (2069 micro strain). Both beams failed suddenly due to inclined major shear crack extending from the left support to the location where the point load was applied.

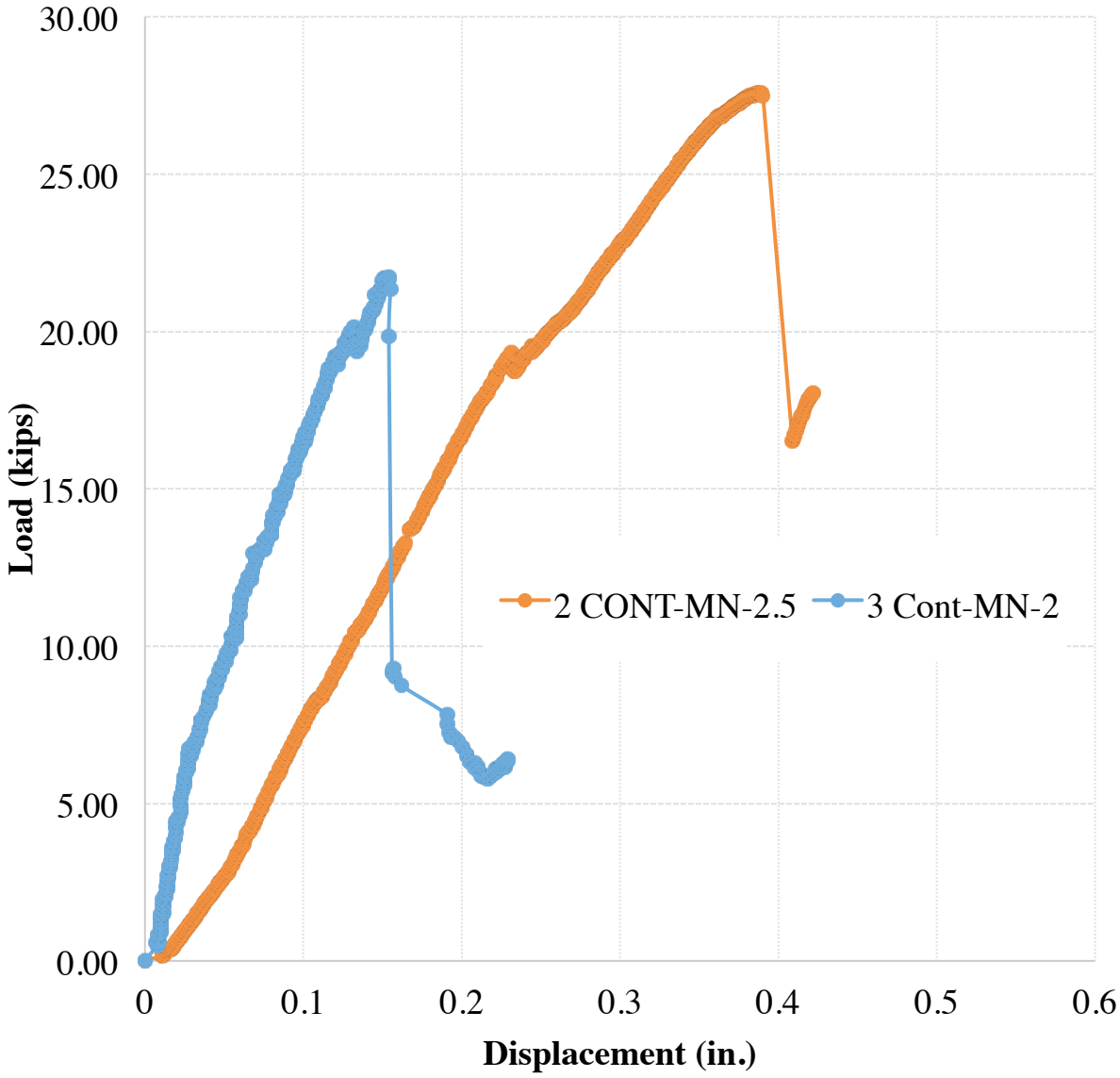

Figure 4.3: Load-Deflection of 2CONT-MN-2.5 and 3CONT-MN-2.

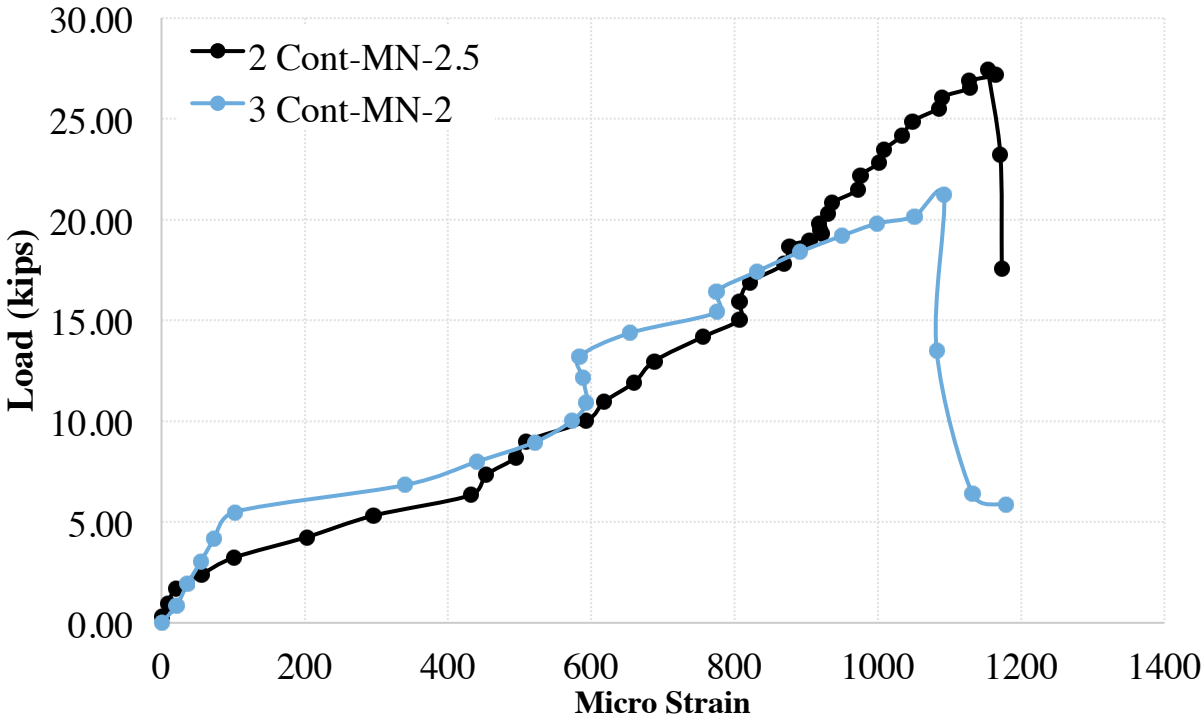

Figure 4.4: Load-Strain history of 2CONT-MN-2.5 and 3CONT-MN-2.

4.2.2 Group 2

The second group of beams had 3 identical specimens made with shear reinforcement. The stirrups were #3 spaced at 8 inches for all beams with 2#5 bottom reinforcement bars. This group of beams was tested with shear spans of 2.0, 2.50, and 3.0. Figures 4.5a shows the crack pattern of beam 4CONT-M8-2 where the first crack started at the bottom-middle of the beam at a load of 5 kips. While the load was increased, the cracks started to propagate toward the neutral axis of the beam at different load steps until a major shear crack suddenly occurred at a load of 21 kips, when the ultimate capacity of the beam was reached. Beam 5CONT-M8-2.5 was tested under a monotonic load with a shear span of 2.5, where the first crack initiated under load of 4 kips. The cracks propagated in a similar way to the previous beam. In this test, the beam did not reach the ultimate capacity due to a sudden displacement

that occurred to the spreader beam during testing. The third beam in this group was designed exactly similar to the previous two beams; however, it was tested under a shear span of 3. The first crack has started at a load level of 7 kips on the tension side of the beam and under continuous loading, cracks propagated until a flexural failure concluded under a load of 30 kips. No sign of shear failure was observed however; some shear cracks observed.

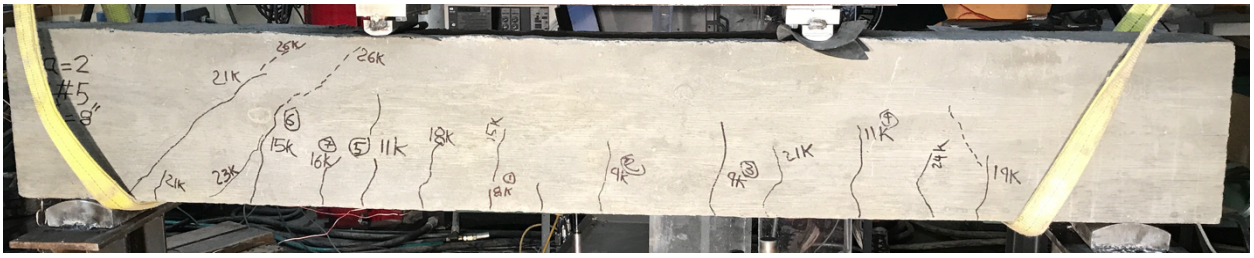

Figure 4.5a: Failure mode of 4Cont-M8-2

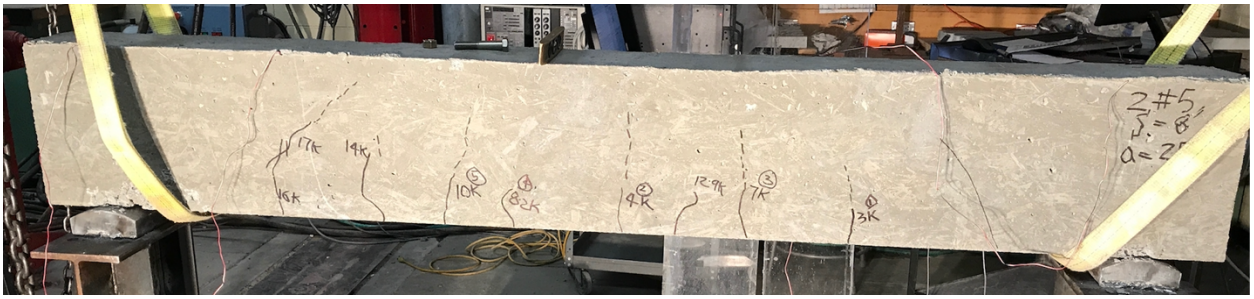

Figure 4.5b: Failure mode of 5Cont-M8-2.5

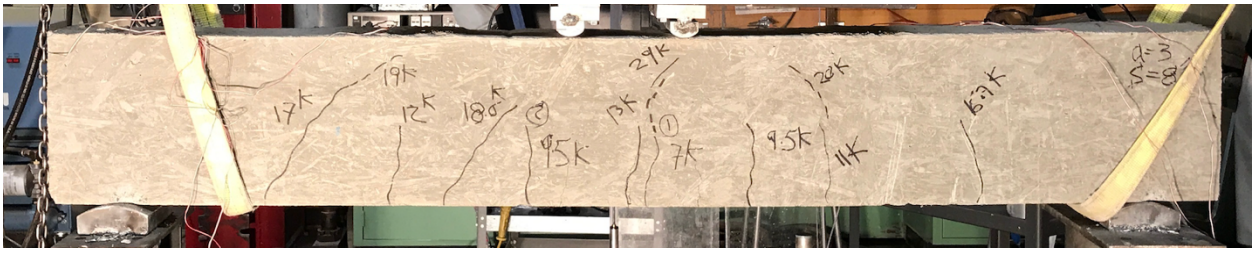

Figure 4.5c: Failure mode of 6Cont-M8-3

The load-displacement of the three beams was recorded and is shown in Figure 4.6. Beam 5CONT-M8-2.5 did not reach the ultimate capacity due to testing malfunction, However the other two beams reached their ultimate capacities.

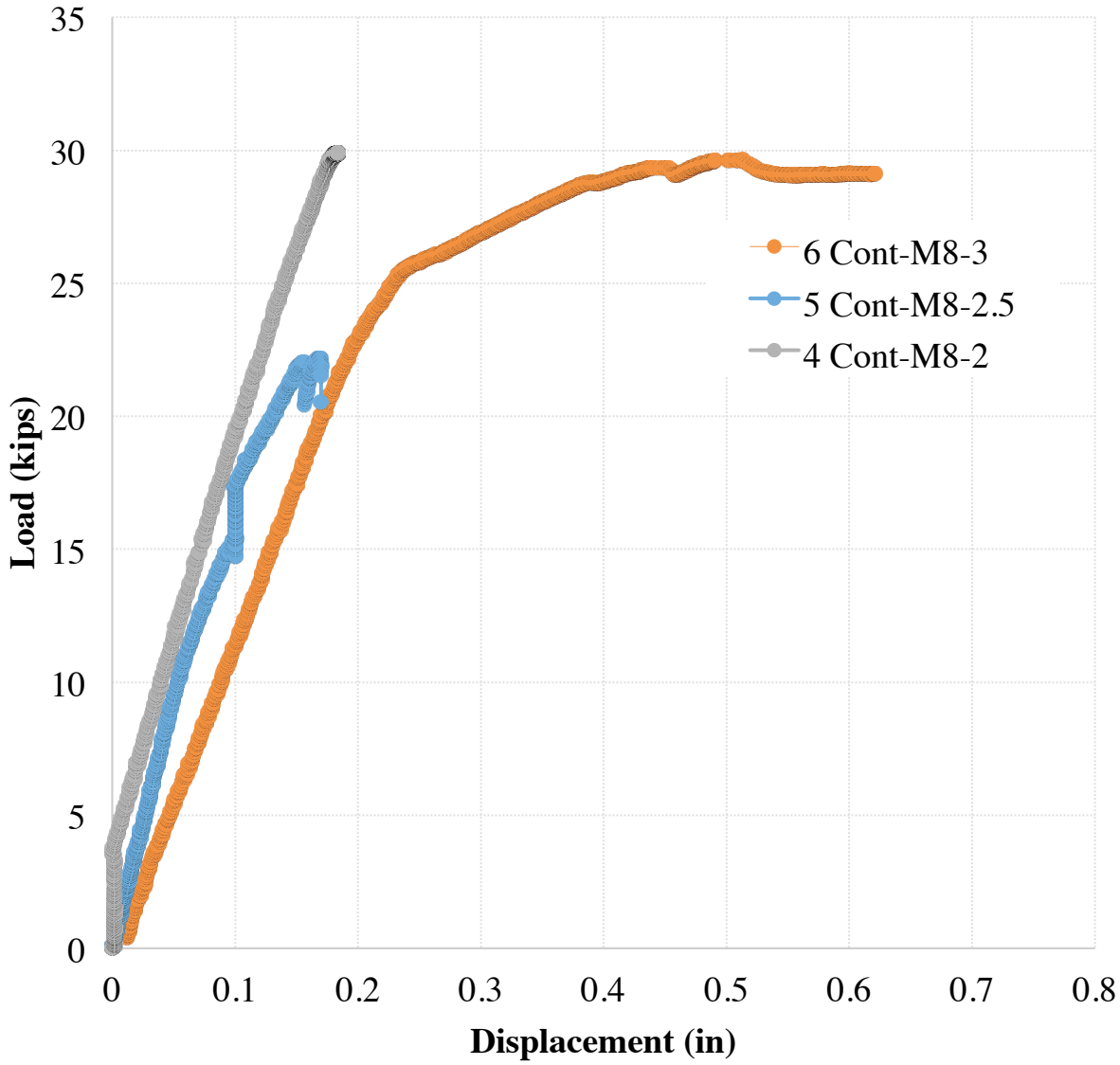

Figure 4.6: Load-displacement of group2.

The load-strain history of the three beams in group 3 recorded and is discussed in the following section. Strain gages were placed on the bottom reinforcement and the stirrup to

capture the behavior under the monotonic load. Figure 4.7a shows the load-strain history of beam 4CONT-M8-2. It can be concluded that the stirrup strain did not reach the yield strain but at a load level of 25 kips, the strain was almost constant and started to decrease when the ultimate load was reached around 29 kips. The strain response of the main reinforcement was increasing as the load was increased until the it reached the ultimate load.

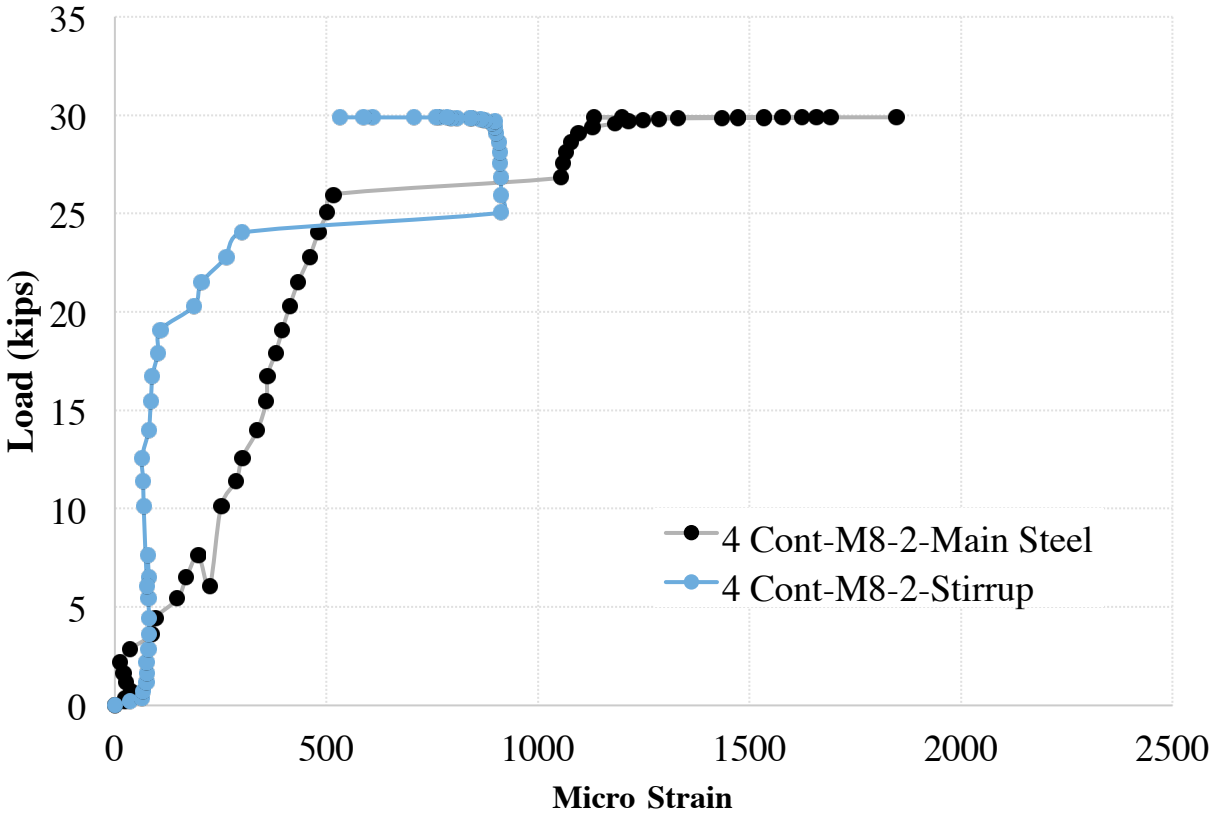

Figure 4.7a: Load-Strain history of 4CONT-MN-2.5

Figure 4.7b shows the load-strain history of beam 5CONT-M8-2.5, where the stirrup strain did not reach the yield strain. The strain response of the main reinforcement was increasing as the load was increased until the it exceeded the yield strain and the test was stopped due to a malfunction.

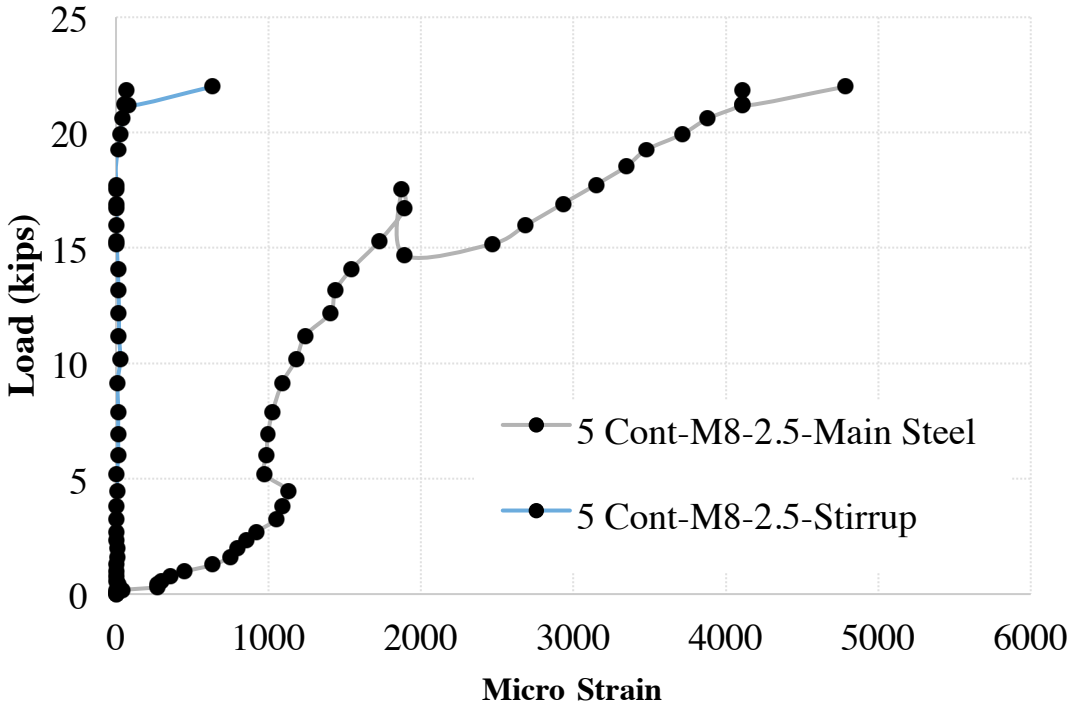

Figure 4.7b: Load-Strain history of 5CONT-MN-2.5 and 3CONT-MN-2.

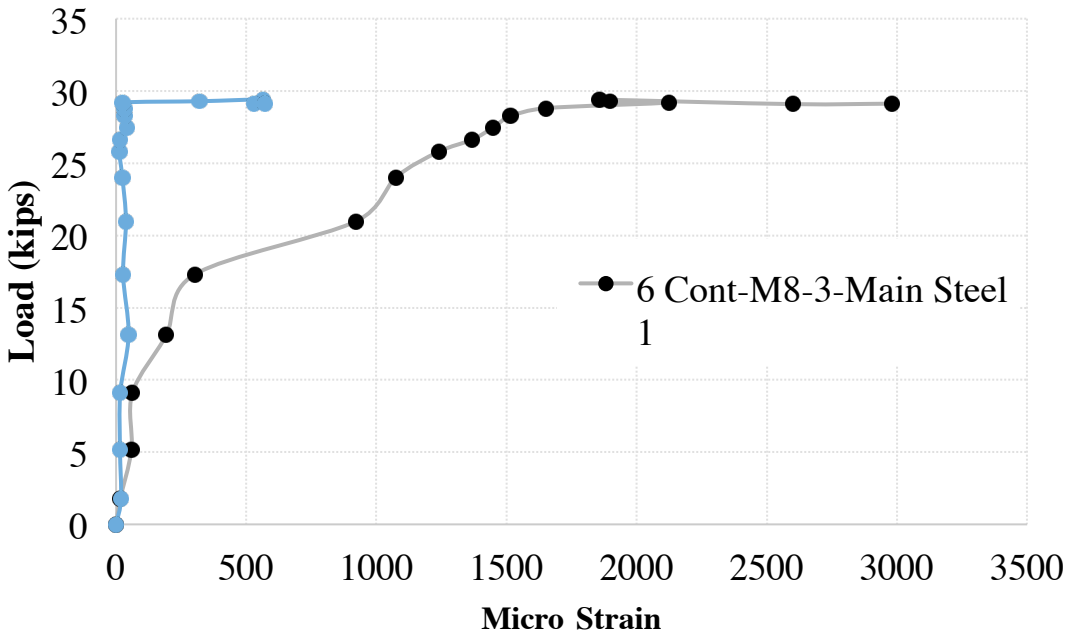

Figure 4.7c: Load-Strain history of 6CONT-MN-3.

4.2.3 Group 3

This group consists of one beam (7Cont-M3-2.5) that has the same characteristics as the previous beams except that it has more stirrups distributed across the beam span (3@3”). The beam was tested under one shear-span-to-depth ration of 3.0. Figure 4.8 shows the failure mode where the beam has reached the ultimate capacity without shear failure, and Figure 4.9 shows the load-displacement response. The cracks were started at a load level of 6.7 kips which the cracks extended until the bottom steel yielded as shown in Figure 4.10.

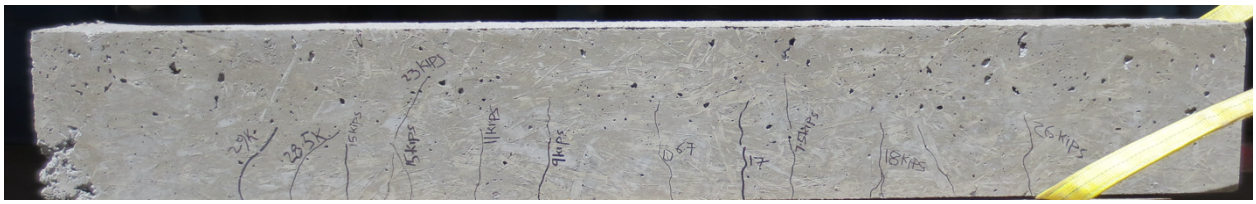

Figure 4.8: Failure mode of 7Cont-M3-2.5

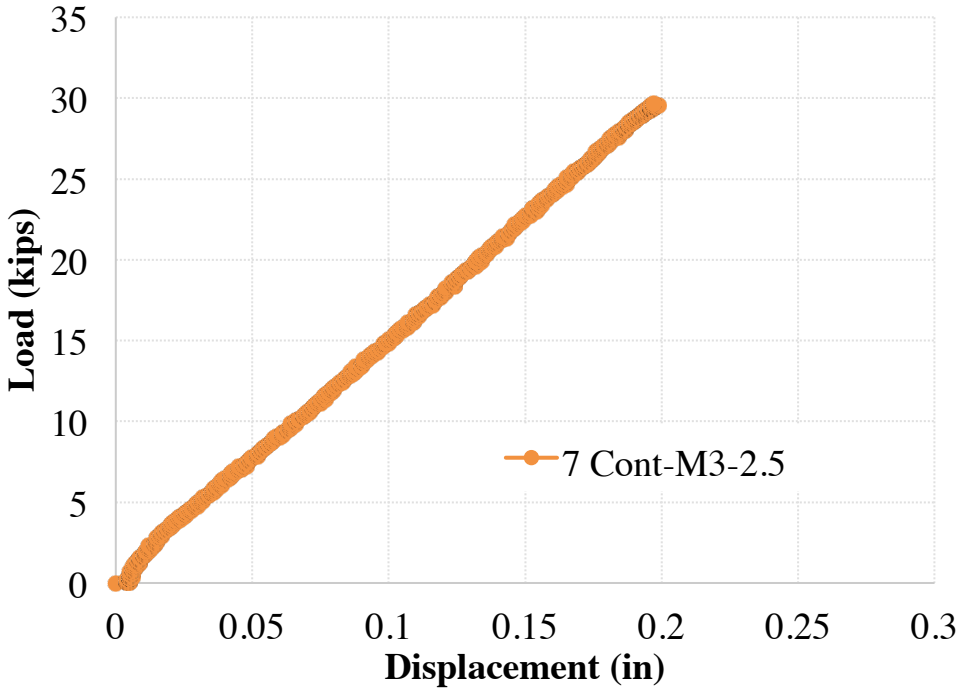

Figure 4.9: Load-displacement of group 3.

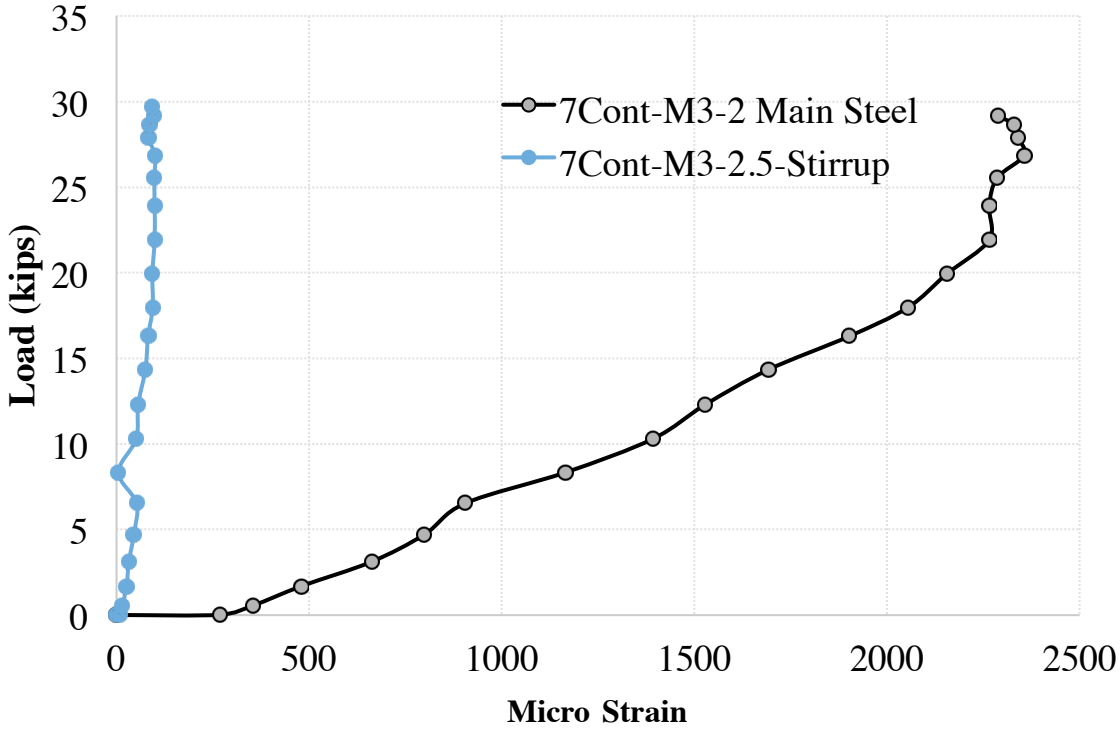

Figure 4.10: Load-Strain history of 7Cont-M3-2.5.

4.2.4 Group 4

Beam 8CF-MN-2.5 beam reinforced with the carbon fiber grid without any shear reinforcement. Two strain gages were attached to the CFRP grid in the tension side. Figure 4.11 shows the expected shear failure mode. The first crack on the tension face occurred at a load level of 5 kips and with increasing the loads, a sudden shear crack occurred close to 29.75 kip. At a load level of 19 kips, a major shear crack started and consequently strain hardening stage started as the load increased. It can be seen in Figure 4.13 that the CRFP grid did not reach the ultimate rupture strain of 14000 micro strain and the concrete failed under shear stresses before the strain reached to ultimate value.

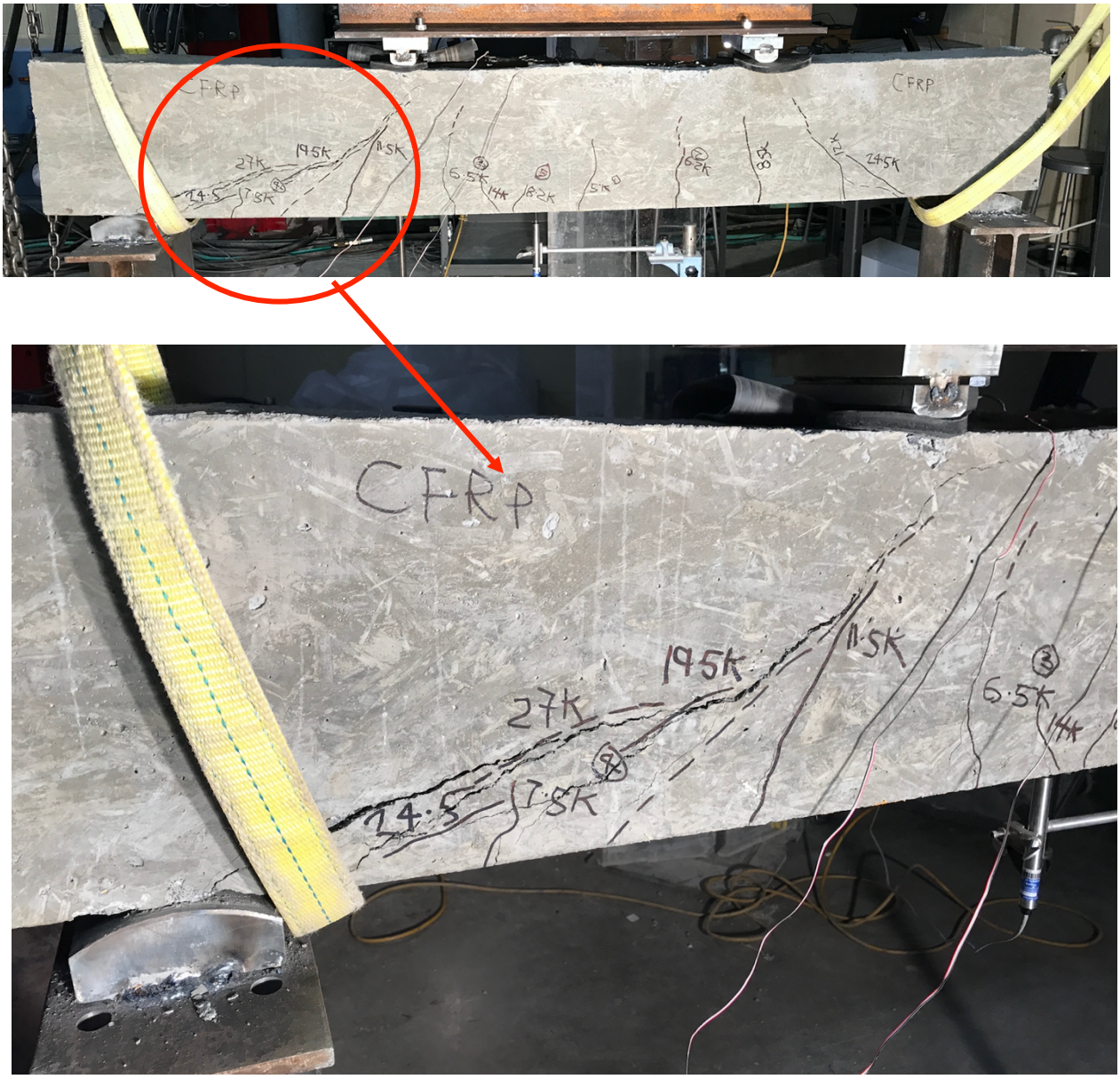

Figure 4.11: Failure mode of 8CF-MN-2.5

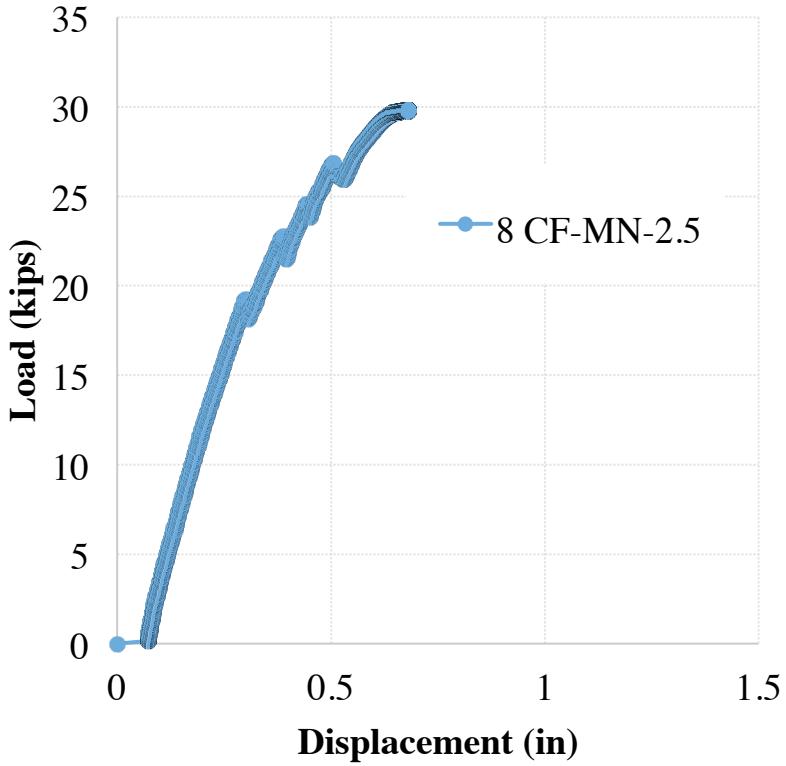

Figure 4.12: Load-displacement of group 4.

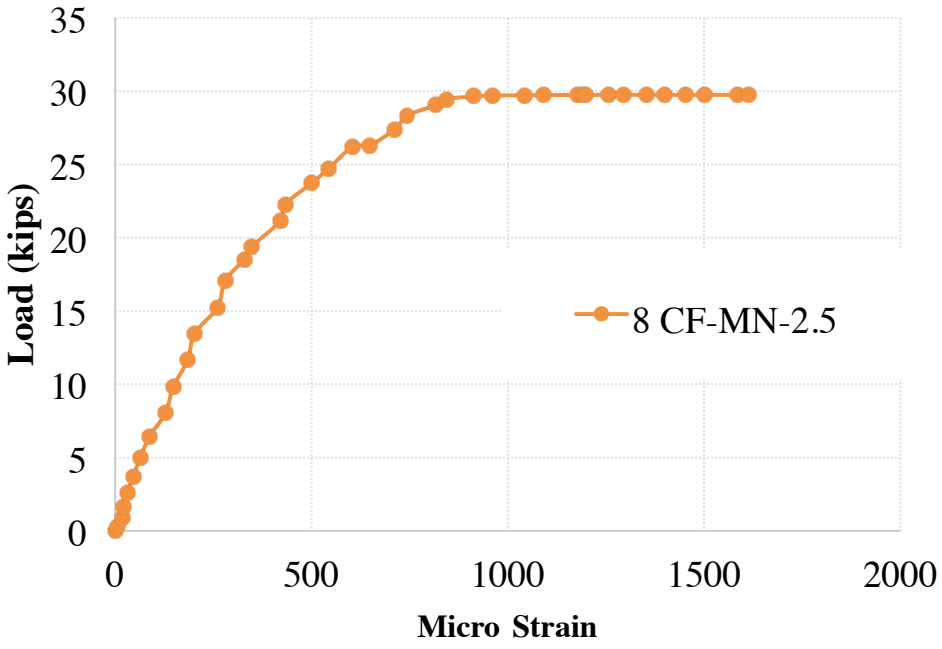

Figure 4.13: Load-Strain history of 8Cont-MN-2.5.

Figure 4.14: Failure mode of 10Cont-MN-2.5.

4.2.5 Group 5

The 10Cont-MN-2.5 beam was reinforced with a glass fiber grid. The beam was tested under a shear span-to-depth ratio of 2.5. The beam started to crack around a load level of 4 kips; the crack was a flexural crack at the mid-span of the beam as seen in Figure 4.14. As the load was increased, the displacement was increased until a sudden shear failure occurred as shown in Figure 4.15. Figure 4.16 shows the load-strain history.

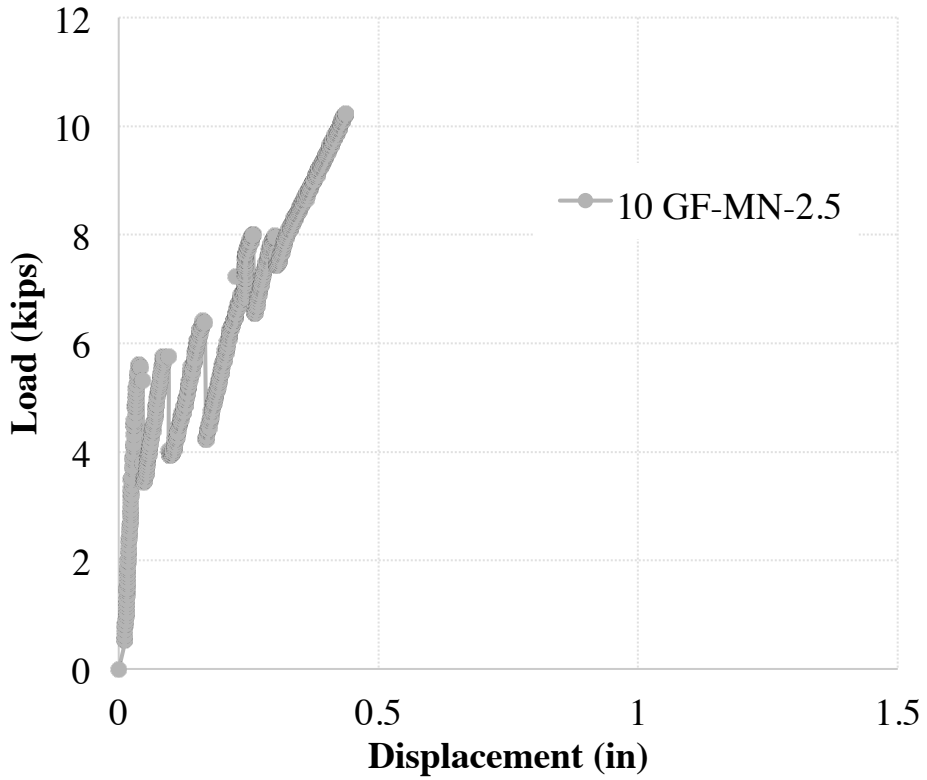

Figure 4.15: Load-Strain history of 10Cont-MN-2.5

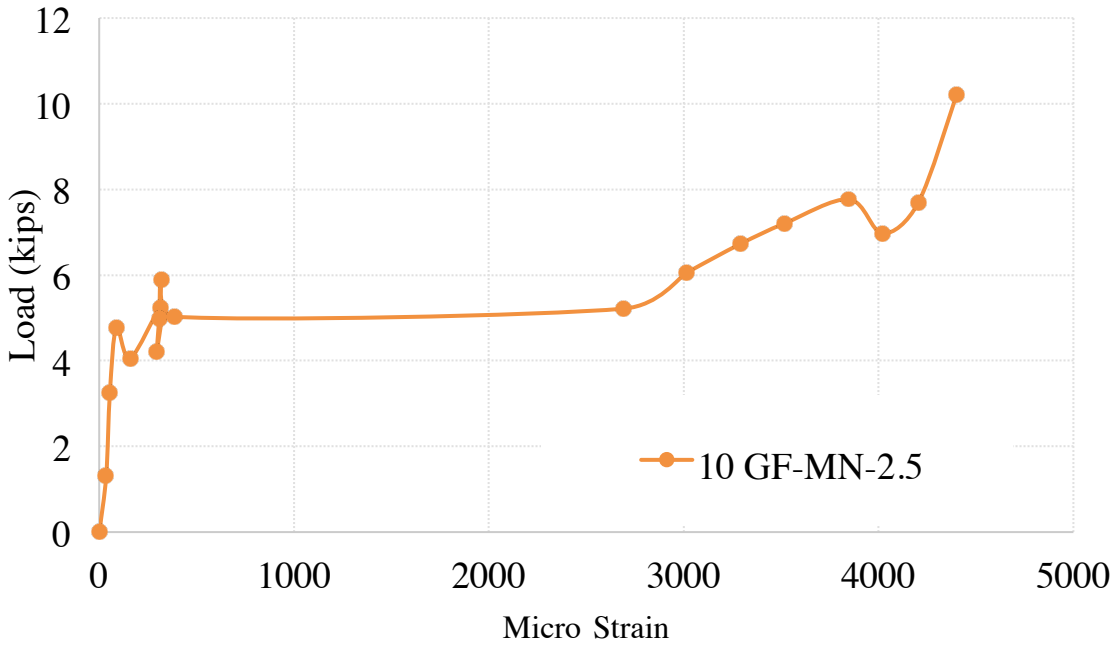

Figure 4.16: Load-Strain history of 10Cont-MN-2.5

All test beams showed significant flexural cracking before inclined cracks joined flexural cracks. Table 4.1 shows the summary of cracking, ultimate loads for all beams and shows also the failure mode and maximum midspan deflection. Table 4.1a shows the summary of the results obtained from the experimental study discussed above.

Table 4.1a: Summary of the results obtained from the experimental study

Specimen	**Flexural Reinforcement Ratio (%)**	**Cracking load, P_{cr} *(Kips)***	***Ultimate Load, (Kips)***	***Max. Deflection Δ_{max} (in.)***	***Failure mode***
2Cont-MN-2.5	0.85	6.0	27.6	0.23	Shear
3Cont-MN-2	0.85	7.5	21.5	0.41	Shear
4Cont-M8-2	0.85	9.0	29.9	0.18	Shear
5Cont-M8-2.5	0.85	4.0	22.2	0.17	Shear-flexure
6Cont-M8-3	0.85	7.0	29.6	0.62	Shear-flexure
7Cont-M3-2.5	0.85	6.7	29.6	0.20	flexure
8CF-MN-2.5	1.0	5.0	29.7	0.68	Shear
10GF-MN-2.5	0.17	4.0	10.5	0.44	Shear

Table 4.1b shows the differences between the cracking moments predicted by the experiments and the values obtained from two codes; ACI 318-16 and ACI 363R-97. The modulus of rupture (f_r) from both codes is not a true indicator of the cracking moment. Cracking moments obtained by f_r, overestimates the actual cracking moment by more than 3 times.

Table 4.1b: Cracking Moment Comparisons

Specimen	Experimental (k.ft.)	ACI 318-16 (k.ft.)*	ACI 363R-97 (k.ft.) **	ACI 318-16/Experiment	ACI 363-16/Experiment
2Cont-MN-2.5	6.88	9.0	13.8	1.50	2.30
3Cont-MN-2	6.88	9.0	13.8	1.20	1.84
4Cont-M8-2	8.25	9.0	13.8	1.00	1.53
5Cont-M8-2.5	4.58	9.0	13.8	2.25	3.45
6Cont-M8-3	9.63	9.0	13.8	1.29	1.97
7Cont-M3-2.5	7.68	9.0	13.8	1.34	2.06
8CF-MN-2.5	5.73	9.0	13.8	1.80	2.76
10GF-MN-2.5	4.58	9.0	13.8	2.25	3.45

*ACI 318-16: $f_r = 7.5\sqrt{f_c'}$
**ACI 363R-97: $f_r = 11.5\sqrt{f_c'}$

4.3 ANALYTICAL PROCEDURES

4.3.1 Stress-Strain Relations

Flexural stress-strain relations are analyzed using the idealized material models as shown in Fig. 4.17. Using Fig. 4.17, the compression zone depth (c), is function of concrete strain ε_c from strain compatibility and internal force equilibrium as follows:

$$c = d\left(\frac{0.003}{0.003+\varepsilon_s}\right) \quad (1)$$

where: ε_c *is concrete strain* ε_s *is the steel strain, and* d *is the beam depth*

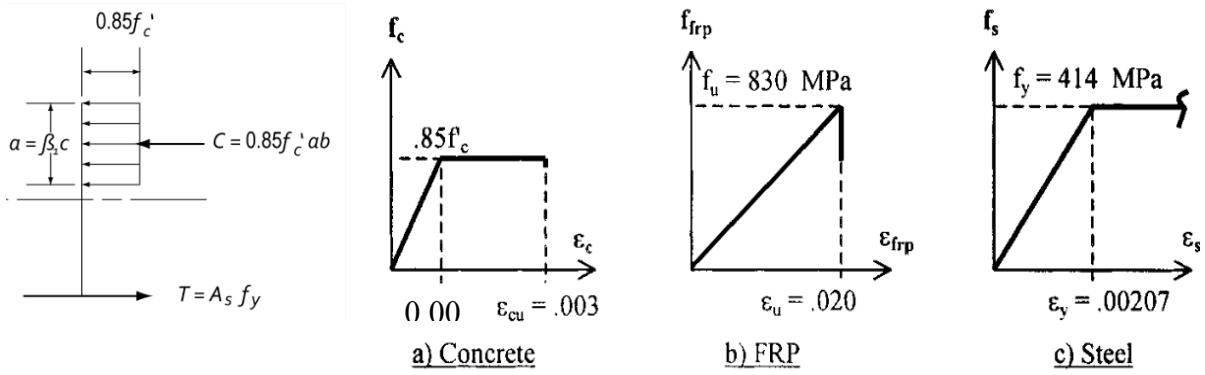

Figure 4.17: Materials models (Yost et al. 2201)

ACI 318-16, the ultimate moment strength can be calculated using a rectangular stress block of constant magnitude $0.85 f'_C$ acting over a depth a (ACI 2016).

$$\beta_1 = \begin{cases} 0.85 & \text{for } f'_c \leq 4{,}000 \text{ psi} \\ 1.05 - 5\times10^{-5}\ f'_c & \text{for } 4{,}000 \text{ psi} < f'_c \leq 8{,}000 \text{ psi} \\ 0.65 & \text{for } f'_c > 8{,}000 \text{ psi} \end{cases} \quad (2)$$

Where, $a = \beta_1 c$ *and* $\beta_1 = 0.65$ for this study based on equation (1) (ACI 318-16)

Finally, the nominal moment strength for beams reinforced with steel bars and corresponding load are calculated using a as shown in (3) through (5). For the FRP grid, equation (7) was used to calculate the FRP stress and equation 8 was used to calculate the nominal moment capacity of beams reinforced with the FRP grids.

$$a = \frac{A_s\ f_y}{0.85\ f'_c b} \quad (3)$$

$$\rho_b = 0.85\beta_1 \left\{\frac{f'_c}{f'_y}\right\}\left\{\frac{\varepsilon_{cu}}{\varepsilon_{cu} + \varepsilon_y}\right\} \quad \text{for Steel} \quad (4)$$

All the tested beams were designed as under reinforced sections.

$$\rho_b = 0.85\beta_1 \left\{\frac{f'_c}{f'_u}\right\}\left\{\frac{\varepsilon_{cu}}{\varepsilon_{cu}+\varepsilon_u}\right\} \quad \text{for FRP} \tag{5}$$

And final the ultimate moment flexural load was calculated based on the below equilibrium equation 6 (ACI 2016).

$$M_n = 0.85\, f'_c ba\left\{d-\frac{a}{2}\right\};\quad P_n^{\text{flex}} = \frac{2M_n}{a_v} \tag{6}$$

$$f_f = \left(\sqrt{\frac{\left(E_f\varepsilon_{cu}\right)^2}{4}} + \frac{0.85\beta_1 f'_c}{\sigma_f}E_f\varepsilon_{cu} - 0.5E_f\varepsilon_{cu}\right) \le f_{fu} \tag{7}$$

$$M_n = 0.85 f_f\left\{d-\frac{a}{2}\right\};\quad P_n^{\text{flex}} = \frac{2M_n}{a_v} \tag{8}$$

Where M_n is the nominal flexural strength (kN.m), a is the depth of equivalent rectangular stress block (mm), f_f is the stress in the FRP bar in tension (MPa), f_{fu} is the design tensile strength of the FRP bar (MPa), E_f is the design or guaranteed modulus (MPa), ε_{cu} is the ultimate strain in concrete (0.003), β_1 is an empirical factor, f'_c is the specified compressive strength of concrete (MPa), ρ_f is the FRP reinforcement ratio, and ρ_b is the balanced FRP reinforcement ratio as given by ACI Committee 440.

For this study, the nominal concrete shear strength of high strength concrete is calculated according to ACI 318-16 and ACI 363R-92. This together with the nominal load at shear failure is given as follows:

$$V_c = \frac{1}{6}\sqrt{f'_c}\, bd \text{ and } \mathrm{v}_{ux} = \left(0.157.\ \sqrt{f'_c} + 17.2.\rho_b.\frac{d}{a}\right) < 0.3\sqrt{f'_c}, \quad (9)$$

$$v_{us} = \frac{A_{sw}}{b.s} f_y \quad (10)$$

$$P_n^{\text{shear}} = 2V_c \quad (11)$$

The modulus of elasticity was calculated based on ACI 363R-92

$$E_c\ = 40{,}000\sqrt{f'_c} + 1{,}000{,}000\ psi \quad (12)$$

Table 4.2 shows the ultimate flexural and shear loads calculated using the ACI 318-16 and compared to the results obtained from the laboratory testing. The maximum difference of 24% between the failure and predicted loads was observed in beam 6Cont-M8-3 and the minimum difference of 3% was observed in beams 4Cont-M8-2 and 7Cont-M3-2.5.

Table 4.2 Comparisons of test results

Sample number	Predicted Strength (kips)		Test Results		Comparison
	P_n^{flex}	P_n^{shear}	Failure	P_{fail}	$P_{fail}/P_{predicted}$
2Cont-MN-2.5	28.79	**26.1**	Shear	27.6	1.06
3Cont-MN-2.0	28.8	**26.1**	Shear	21.5	0.82
4Cont-M8-2.0	**28.79**	62.0	Shear	29.9	1.03
5Cont-M8-2.5	**28.1**	62.0	Shear-flexure	22.2	0.80
6Cont-M8-3.0	**23.9**	123	Shear-flexure	29.6	1.24
7Cont-M3-2.5	**28.8**	62.0	flexure	29.6	1.03
8CF-MN-2.5	64.5	**26.1**	Shear	29.7	1.13
10GF-MN-2.5	**12.13**	26.1	Shear	10.5	0.86

4.3.2 Deflection Prediction

The elastic bending theory, load-point flexural deflection Δ_a for the test setup in is calculated from:

$$\Delta_a = \frac{1}{24}\{3L^2 - 4a^2{}_v\}\left(\frac{M_a}{I_e E_c}\right) \quad (13)$$

Where $\boldsymbol{M_a}$=applied moment; $\boldsymbol{E_c}$=concrete elastic modulus calculated as per ACI 318-16 (equation 12), and $\boldsymbol{I_e}$=effective moment of inertia specified in ACI 318-16 based on the Branson equation (1965), as follows:

$$I_e = \left(\frac{M_{cr}}{M_a}\right) I_g + \left\{1 - \left(\frac{M_{cr}}{M_a}\right)^3\right\} I_{cr} \quad (14)$$

In (14), I_{cr} and I_g are the cracked and gross moment of inertia respectively, and M_{cr} is the cracking strength determined for gross section properties and rupture strength from ACI 318-16, Note that $I_e$represents the parabolic ‘‘Branson’’ equation and is assumed constant over the beam length L. Equation 10 was used to predict the deflection at the midspan of all beams including the those reinforced with FRP grids. Other equations such as were used such as Benmokrane et a. 1996, ACI-440-15 and ACI-440-06 to compare the deflection calculated of beams reinforced with FRP grids. The equations used are 15 to 17.

Benmokrane et a. 1996 equation (11) modified the main Branson equation to make it suitable for FRP-reinforced concrete beams and it is based on experimental data.

$$Ie = \left(\frac{M_{cr}}{M_a}\right)^3 * \frac{I_g}{\beta} + \alpha \left[1 - \left(\frac{M_{cr}}{M_a}\right)^3\right] I_{cr} \leq I_g \quad (15)$$

The noticeable difference lies in the modification of α and β. α reflects the reduced composite action between the concrete and FRP bars. However, β has no physical significance because there was no justification for reducing Ig. α and β were 0.84 and 7,

respectively.

ACI 440.1R-06 recommended an equation for the effective moment of inertia based on Branson's model. There was an additional factor for considering the reduced tension stiffening of FRP-reinforced concrete members. This model has been commonly used to calculate the moment of inertia of FRP-reinforced concrete members, so that the deflection of the cracked section can be calculated:

$$Ie = \left(\frac{M_{cr}}{M_a}\right)^3 \beta_d * I_g + \left[1 - \left(\frac{M_{cr}}{M_a}\right)^3\right] I_{cr} \leq I_g, \qquad (16)$$

Where β_d is the reduction factor related to the reduced tension stiffening exhibited by R/C member with FRP bar, β_d = (1/5) (ρ_f/ρ_{fb}) ≤ 1.0), ρ_f is the reinforcement ratio of the FRP bar, and ρ_{fb} is the balanced reinforcement ratio of FRP grid.

ACI 440.1R-15 suggested an equation for calculating the effective moment of inertia for reinforced concrete beams with FRP bars. This equation is based on Bischoff's proposed approach, which represents a weighted average of flexibility along beam span (1/E), as shown in (13 and 14). It was reported that the equation works equally well for both steel-and GFRP-reinforced concrete members with no empirical parameter [Bisscoff 2005].

$$I_e = \frac{I_{cr}}{1 - \gamma \left(\frac{M_{cr}}{M_a}\right)^2 [1 - I_{cr/I_g}]} \leq I_g \, , \qquad (17)$$

where γ is the parameter to account for the variation in stiffness along the length of the member for four-point bending. Hence,

$$\gamma = \frac{3\left(\frac{a}{L}\right) - 16\left(\frac{M_{cr}}{M_a}\right)\left(\frac{a}{L}\right)^2 + 12\left(\frac{a}{L^3}\right)}{3\left(\frac{a}{L}\right) - 4\left(\frac{a}{L^3}\right)}, \quad (18)$$

4.4 COMPARATIVE STUDY FOR THE PREDICTION OF DEFLECTION BEHAVIOR

4.4.1 Group 1

In this study, the effective moment of inertia of eight high strength concrete beams reinforced with various reinforcements were compared and analyzed. The comparative study of the effective moment of inertias was based on Branson's equation 1965, Benmokrane et a. 1996, ACI 440.1R-15, and ACI 440.1R-06 and compared to the experimental tests. Some studies showed that the evaluation of structural capacity of FRP bar-reinforced concrete beam using only one representative specimen for each reinforcing group was successfully done, Barris et al. (2009), and Noe et al. (2014).

Figure 4.18a shows of the applied moment versus the effective moment of inertia of group 1 using Branson's equation. Group 1 is reinforced with conventional steel bars (2#5) with no shear reinforcement and the only difference was the shear span-to-depth ratio (a/d) (2.0 and 2.5). It can be seen that (a/d) showed a negligible effect in predicting the effective moment of inertia. Figure 4.18b shows a comparison between the load-displacement history of group 1. Both analytical and experimental results showed relatively good agreement in terms of the ultimate load and maximum displacement for beams 2CONT-MN-2.0 and 3CONT-MN-2.5. As expected, Branson's analytical model showed more overall stiffness behavior before and after the cracking moment for beam 2CONT-MN-2.0; however, that was not the case for 3CONT-MN-2.5, where Branson's equation underestimated the displacement at the same load level.

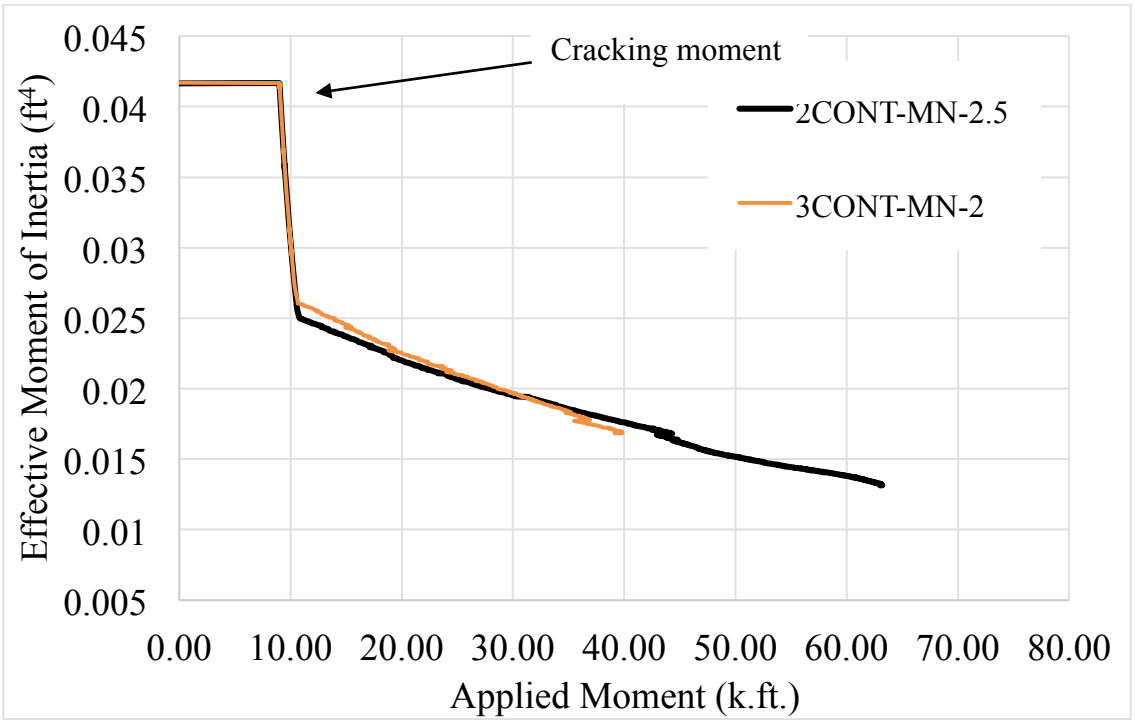

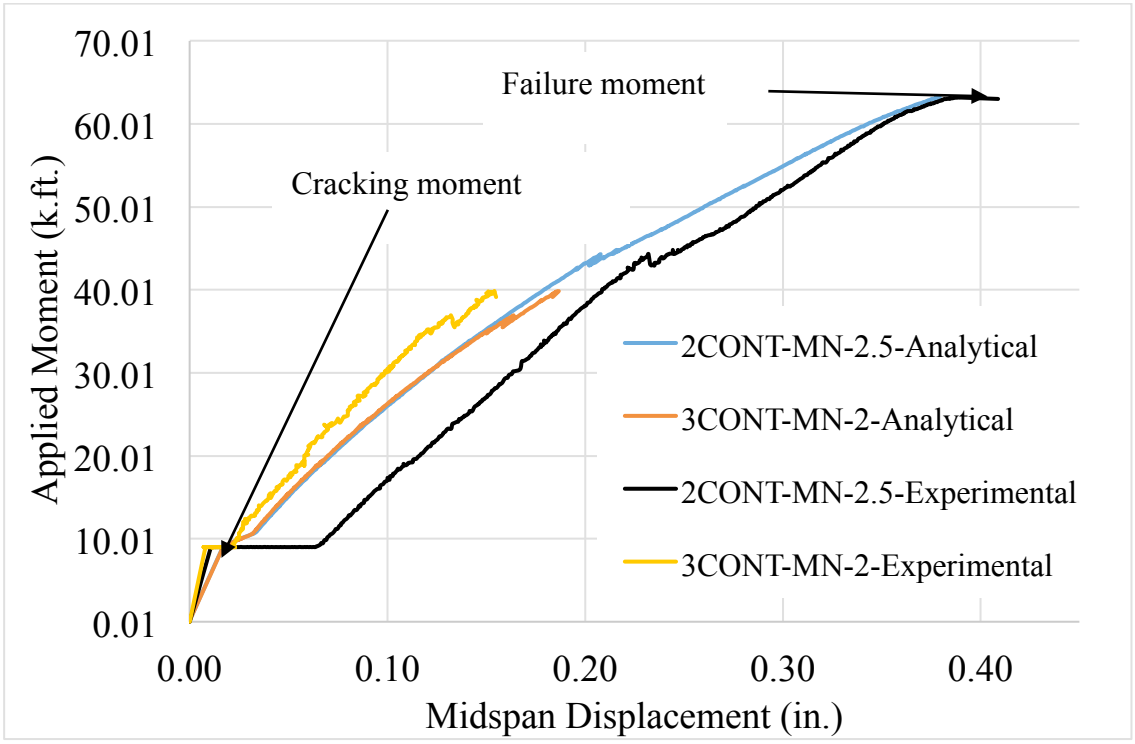

Figure 4.18: a) Effective moment of inertia of group 1, b) moment-displacement of group 1.

4.4.2 Group 2

Figure 4.19a shows the results of the applied moment versus the effective moment of inertia of group 2 using Branson's equation. Group 2 is reinforced with conventional steel bars (2#5) with #3 stirrups spaced equally at 8 inches. The shear span-to-depth ratio (a/d) was 2.0, 2.5, and 3.0 for beams 4CONT-M8-2, 5CONT-M8-2.5, and 6CONT-M8-3, respectively. The (a/d) ratio has a noticeable effect on the effective moment of inertia results as shown in Fig. 4.18a. The behavior of all three beams were same when the applied moment was zero and up to the cracking moment (9 k.ft.). When the applied moment exceeded the cracking moment a sudden drop in the effective moment of inertia was observed. The beam with (a/d) = 2.5 showed the highest decrease in the effective moment of inertia while the beam with (a/d) =3.0 showed the lowest decrease in effective moment of inertia. In figure 4.18b, the beam with a/d=3 (6CONT-M8-3) showed the highest ultimate moment (79.41 k.ft. for the analytical model and 81.5 k.ft. for the experimental results), however as shown; Branson's equation over- predicted the deflection due to the lower stiffness behavior. For example, at an applied moment of 70 k.ft, the deflection values were 0.187 in. and 0.348 in for the analytical and experimental results, respectively with an overestimation percentage of 86%. Same behavior was observed in beams 4CONT-M8-2, 5CONT-M8-2.5 where the analytical solution overestimated the deflection at the same moment applied. For beam 4CONT-M8-2, the ultimate deflection obtained from the analytical model was 39.6% compared to the experimental deflection, while for beam 5CONT-M8-2.5, the ultimate deflection obtained from the analytical model was 61.6% compared to the experimental deflection.

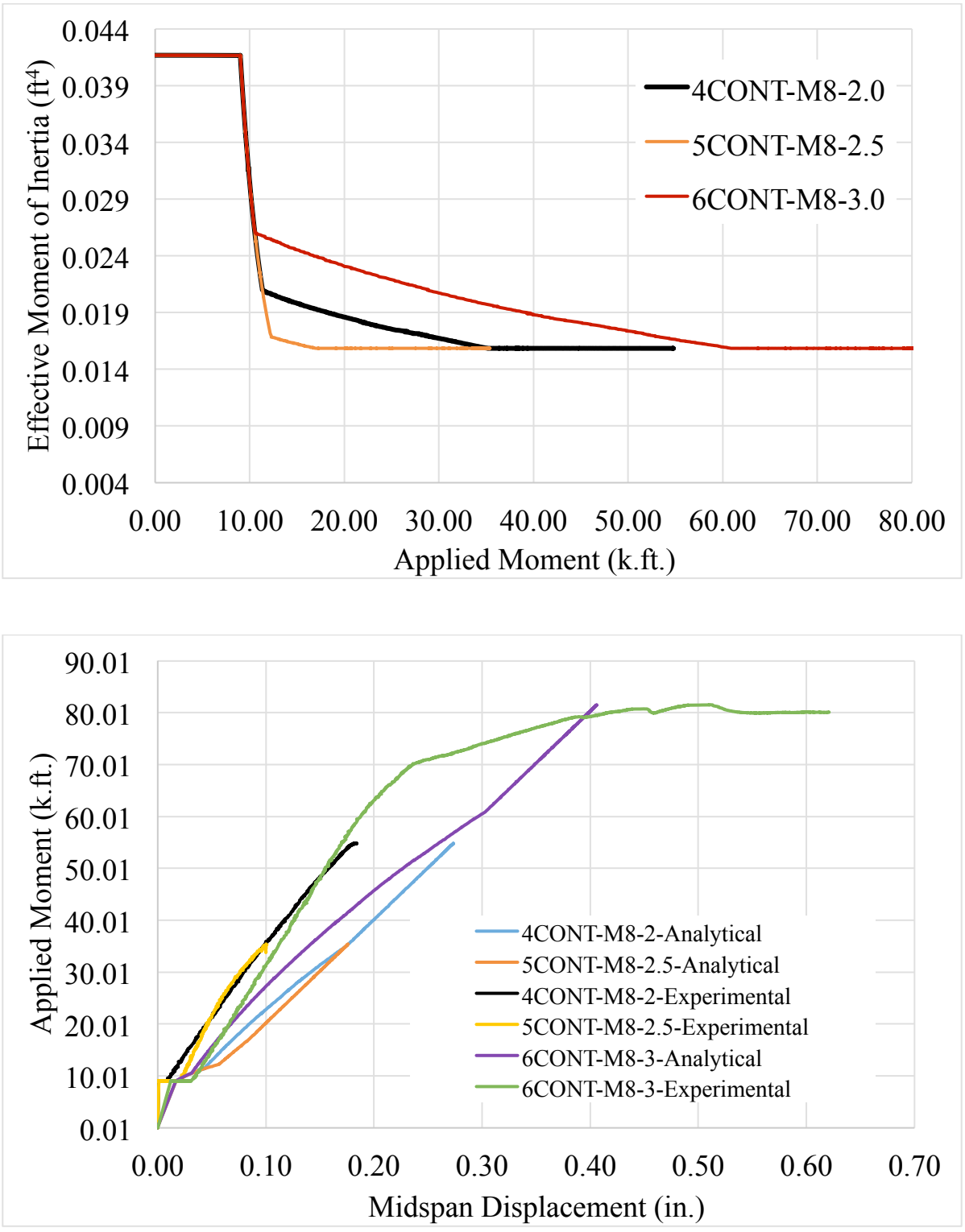

Figure 4.19: a) Effective moment of inertia of group 2, b) load-displacement of group 2.

4.4.3 Group 3

Group 3 consisted of two reinforced concrete with one beam reinforced with #3 stirrups spaced equally at 8 inches and the other beam reinforced with #3 stirrups spaced at 3 inches. The two beams 5CONT-M8-2.5 and 7 CONT-M3-2.5 had the same (a/d) ratio of 2.5. The (a/d) ratio has a significant effect on the effective moment of inertia results as shown in Fig. 4.20a. The behavior of the two beams were same when the applied moment was zero and up to the cracking moment (9 k.ft.). When the applied moment exceeded the cracking moment, a sudden drop in the effective moment of inertia was observed. Beam 5CONT-M8-2.5 showed a higher decrease in the effective moment of inertia compared to beam 7 CONT-M3-2.5 with the heavier shear reinforcement.

In figure 4.20b, beam 7CONT-M3-2.5 showed higher ultimate moment (68.1 k.ft. for the analytical model and 67.6 k.ft. for the experimental results), however as shown in Fig. 4.20b, Branson's equation over predicted the deflection. The ultimate deflection values of 7CONT-M3-2.5 were 0.337 in. and 0.197 in. for the analytical and experimental results, respectively with an overestimation percentage of 71%. The same behavior was observed in beams 5CONT-M8-2.5 where the analytical solution overestimated the failure deflection by 71.5% (0.175 inch from the analytical versus 0.102 inch from the experiment).

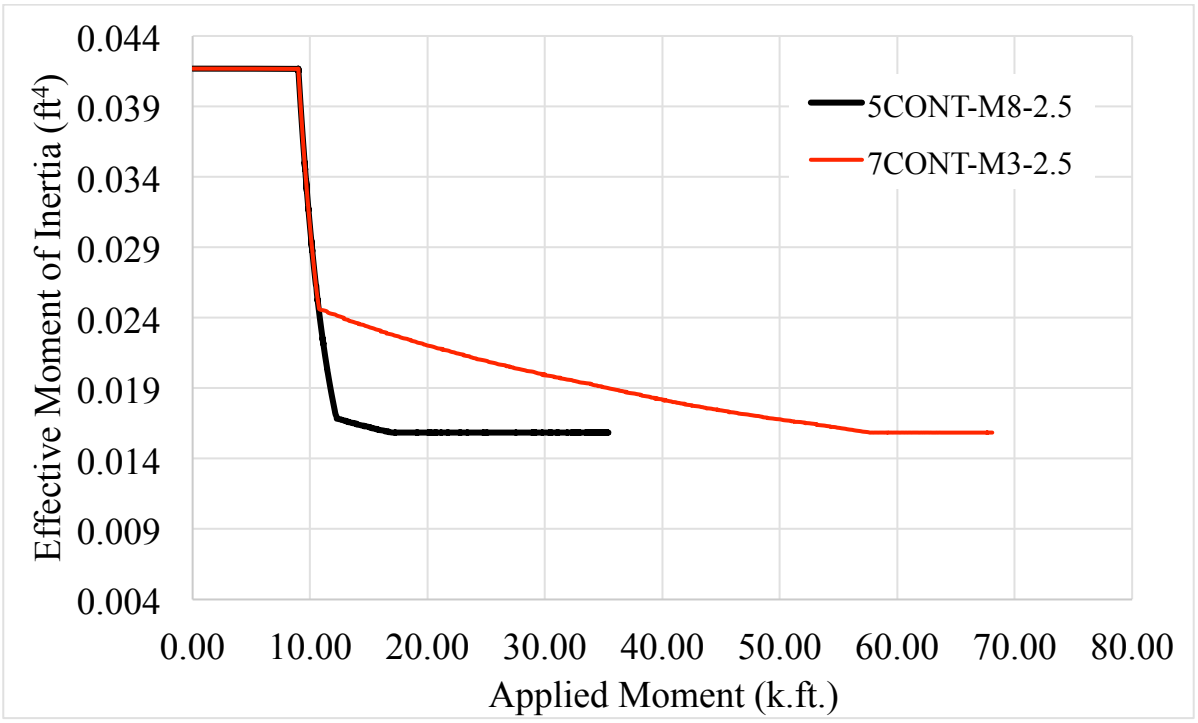

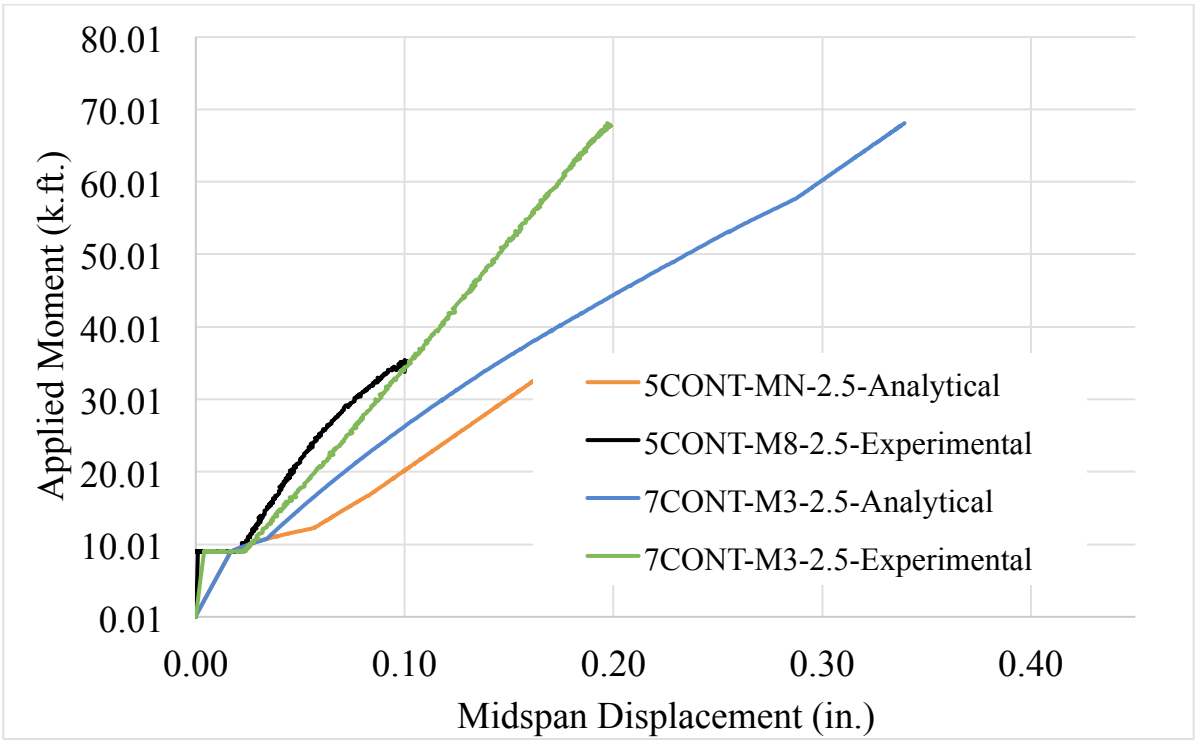

Figure 4.20: a) Effective moment of inertia of group 3, b) load-displacement of group 3.

4.4.4 Group 4

Group 4 consisted of one reinforced concrete beam (8CF-MN-2.5) reinforced with CFRP grid without stirrups. Some studies showed that the evaluation of structural capacity of FRP bar-reinforced concrete beam using only one representative specimen for each reinforcing group was successfully done [Barris et al. (2009), and Noe et al. (2014)]. The beam had an (a/d) ratio of 2.5. The deflection of the beam was predicted using four different analytical models (Branson et al. 1965, Benmorkane et al. 1996, ACI 440.1R-06, and ACI 440.1R-15). Figure 4.21a presents the effective moment of inertia versus the applied moment for the four models.

The behavior of the beam using the four models were the same when the applied moment was zero and up to the cracking moment (9 k.ft.). When the applied moment exceeded the cracking moment a sudden drop in the effective moment of inertia was observed. The models developed by Benmorkane et al. 1996, and ACI 440.1R-06 showed the same behavior and as shown to differentiate between the two-model's response in Figure 4.21a. The ACI 440.1R-15 model showed a different decrease in the I_e especially when the applied moment reached a value of 11.58 k.ft., where the I_e increased suddenly and then maintained a constant value up to the beam failure. The Branson et al. 1965 model showed very different behavior where the model showed higher effective moment of inertia compared to the other three models at the same applied moment level.

In figure 4.21b, beam 8CF-MN-2.5, all the four models under-predicted the load-

displacement history compared to the experimental results. There was no significant difference in the load-displacement values between the four models themselves. At the ultimate load, the experimental deflection value was 0.68 in. compared to almost 0.26 for the four analytical models, which shows an overestimation of 261%.

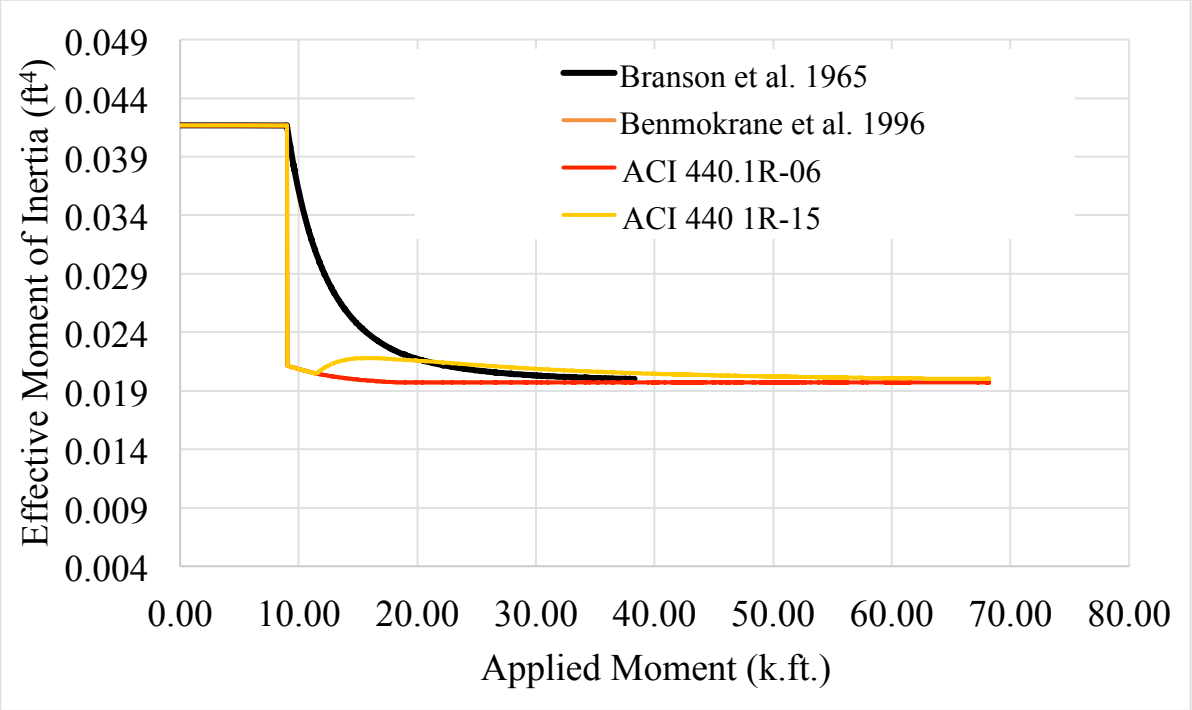

Figure 4.21: a) Effective moment of inertia of group 4

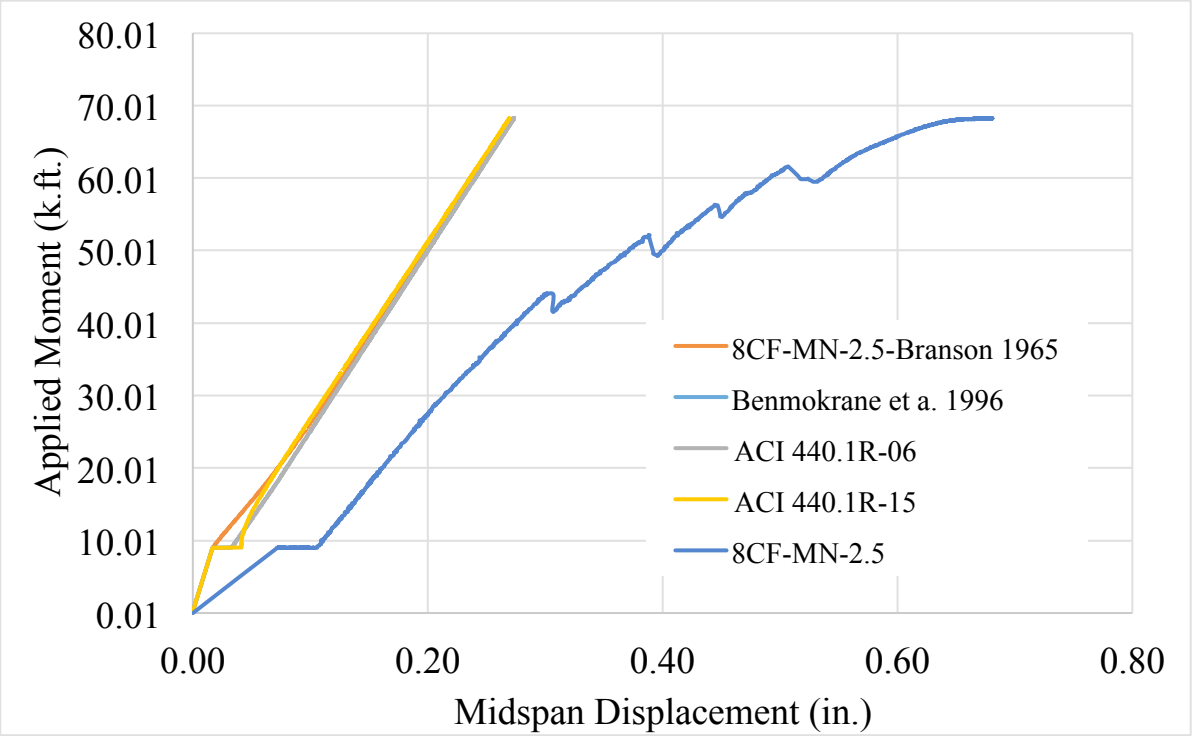

Figure 4.21: b) load-displacement of group 4.

4.4.5 Group 5

Group 5 consisted of one reinforced concrete beam (10GF-MN-2.5) reinforced with GFRP grid without shear reinforcement. The beam had a (a/d) ratio of 2.5. the deflection of the beam was predicted using four different analytical models (Branson et al. 1965, Benmorkane et al. 1996, ACI 440.1R-06, and ACI 440.1R-15). Figure 4.22a presents the effective moment of inertia versus the applied moment for the four models.

The behavior of the beam using the four models were the same when the applied moment was zero and up to the cracking moment (9 k.ft.). When the applied moment

exceeded the cracking moment a sudden drop in the effective moment of inertia was observed. The models developed by Benmorkane et al. 1996, and ACI 440.1R-06 showed similar in behavior as shown in 4.22a. The ACI 440.1R-15 model showed different decrease in the I_e. The Branson et al. 1965 model showed very different behavior where the model showed higher effective moment of inertia compared to the other three models at the same applied moment level. The oscillations in the experimental data shown in Figure 4.22 is attributed to the concrete failure and GFRP delamination during testing.

In figure 4.22b, all four models under-predicted the load-displacement history compared to the experimental results. There was no significant difference in the load-displacement values between the four models themselves. At the ultimate load, the experimental deflection value was 0.673 in. Compared to almost 0.174 for the four analytical models, which shows an overestimation of 387%.

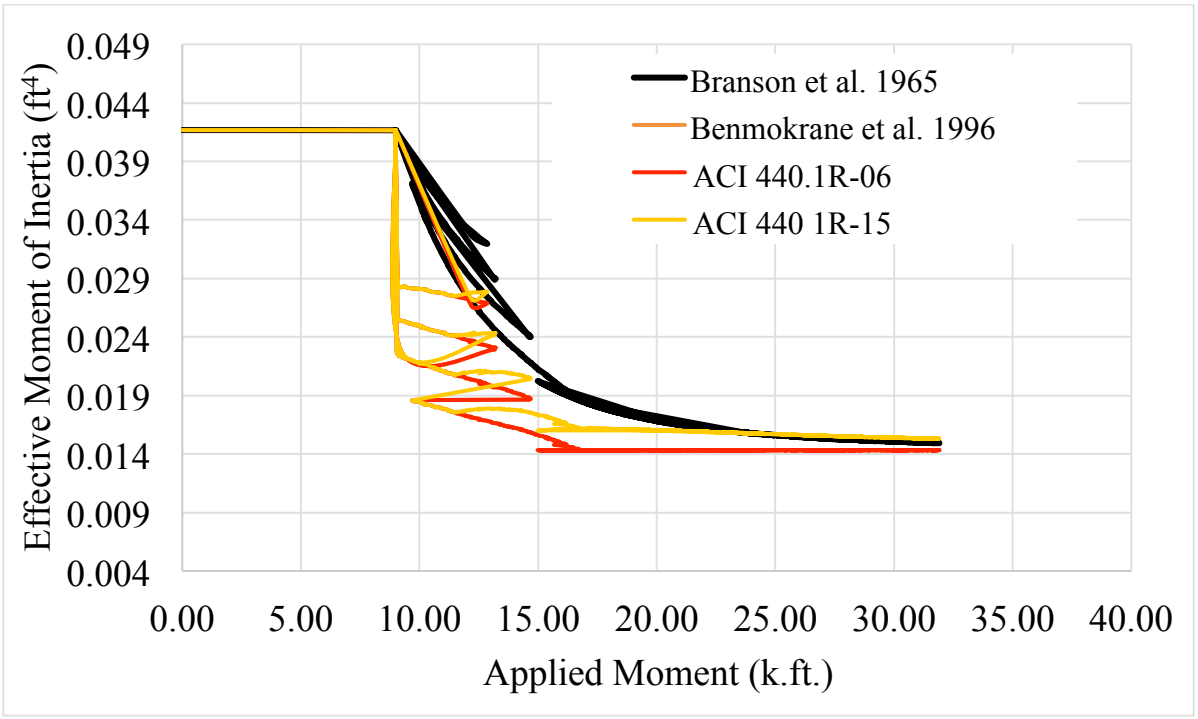

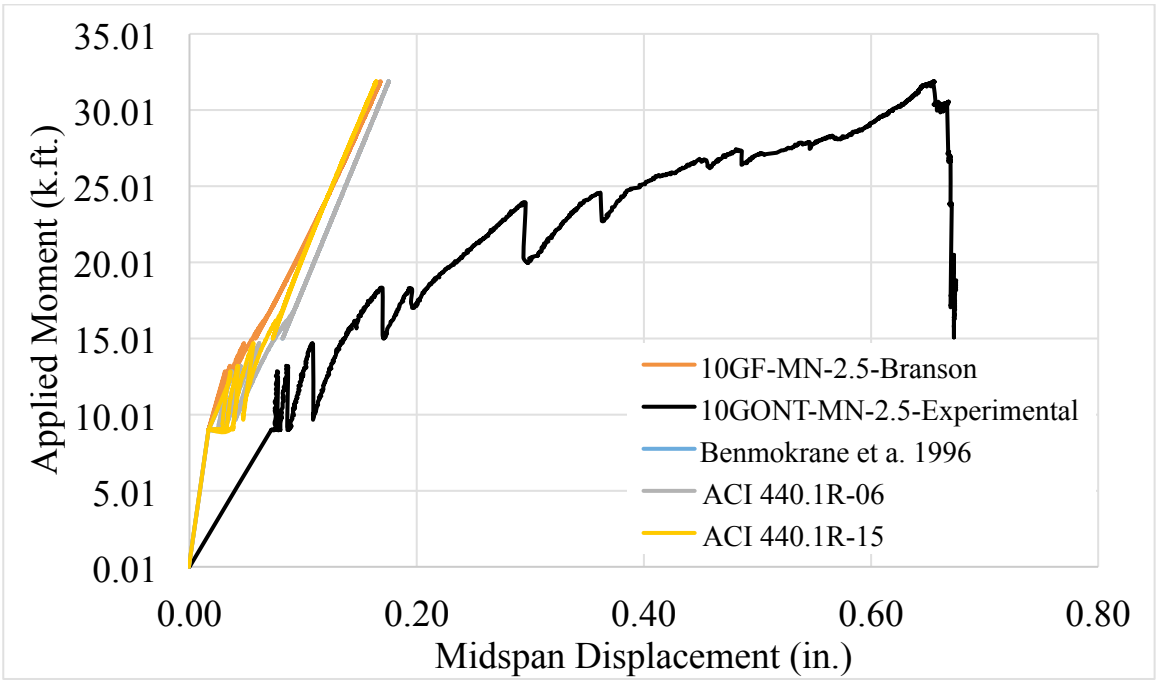

Figure 4.22: a) Effective moment of inertia of group 5, b) load-displacement of group 5.

4.5 Comparative Study between the Steel, CFRP, and GFRP Reinforcement

Figure 4.23a shows the analytical and experimental load-deflection history for beam 2CONT-MN-2.5 and 8CF-MN-2.5. As predicted the carbon fiber grid showed lower stiffness compared to the steel bars due to the lower modulus of elasticity of the CF grid compared to the steel bars. Therefore, CF grid showed more deflection at the ultimate load.

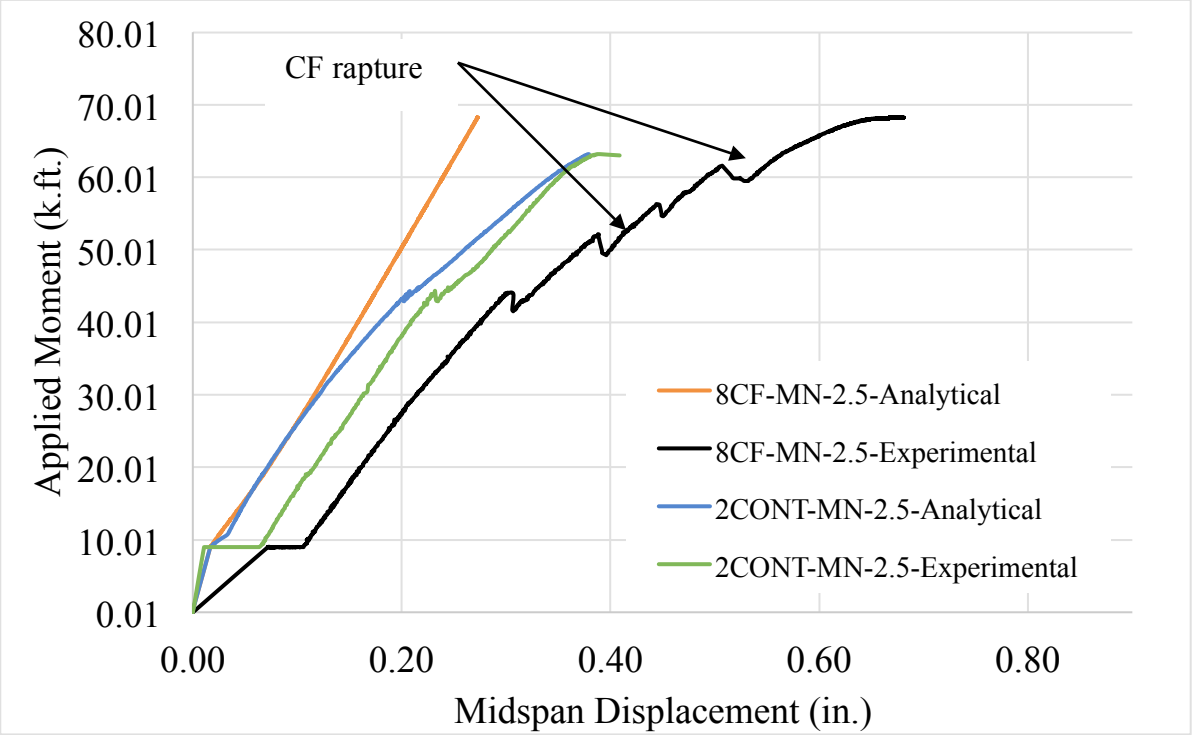

Figure 4.23a: Comparison between the steel and CF grid behavior

Figure 4.23 b shows the analytical and experimental load-deflection history for beam 2CONT-MN-2.5 and 10GF-MN-2.5. The stiffness of the glass fiber grid is lower than the corresponding value of steel reinforced beams. Additional research is necessary to establish appropriate service stress limits, strength reduction factors. Finally, the greater cross-sectional area of the CF and GF grids, compared to steel reinforcements, requires that

reinforcement anchorage provisions be considered. design details.

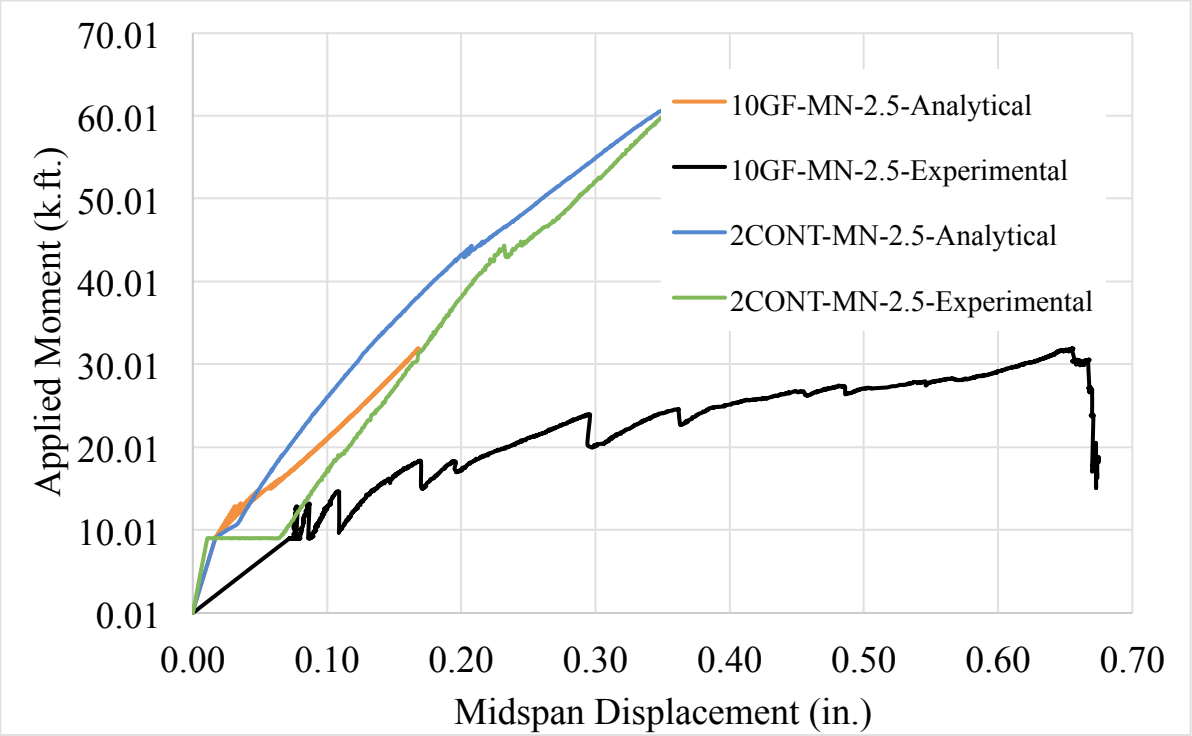

Figure 4.23b: Comparison between the steel and CF grid behavior

CHAPTER 5: SUMMARY AND CONCLUSIONS

The main goal of this study is to investigate the behavior of high strength concrete beams reinforced with various reinforcement under monotonic loading with various shear span-to-depth ratio and to compare the measured load-deflection history with the available prediction equations. In this study, eight high strength concrete (HSC) beams were prepared and cast using a concrete with a strength of 10 ksi. All beams were 7 ft. span and 12 inches depth and 6 inches width. Some of beams were reinforced with conventional #5 steel bars and others were reinforced with carbon fiber (CF) and glass fiber grids. Three beams were reinforced with #3 stirrups at 8 inches spacing and one beam was reinforced with #3 stirrups at 3 inch spacing. The beams were simply supported and subjected to a monotonic four-point bending load using servo-valve actuator with a capacity of 75 kips under three shear span-to-depth ratio.

The data collected in this study included load-displacement-history at midspan, steel and carbon fiber strains, mode of failure and crack patterns. Limited data were found on the literature on the behavior of high strength concrete beams reinforced with carbon and glass fiber grids. The experimental results were compared to analytical models from the literature. The models predict the effective moment of inertia of reinforced concrete beams and consequently predict the deflection at the cracking and at the ultimate loads.

The study concluded that the behavior of the HSC beams was dependent on the type of reinforcement and on the shear span-to-depth ratio as well as the availability of transverse reinforcement. The analytical models, predictions of failure ultimate loads and mode of failure were in good agreement with the experimental results. For the HSC beams reinforced

with steel bars, Deflections calculated using Branson's effective moment of inertia overestimated the deflection and for beams reinforced with CFRP and GFRP grids, the analytical effective moment of inertia equations developed by ACI 440.1R-06, ACI 440.1R-15, and Benmorkane et al. 1996) under estimated the deflection at the midspan and that concludes the need to modify the existing deflection equations when HSC reinforced with carbon fiber grids.

The following specific conclusions were drawn from the present study:

- It is feasible to use the CFRP and GFPG as a reinforcement in high strength concrete beams.
- The modulus of rupture from both codes is not a true indicator for the cracking moment. Cracking moments obtained by the modulus of rupture, overestimates the actual cracking moment by more than 3 times.
- A maximum difference of 24% between the failure and predicted loads was observed in beam 6Cont-M8-3 and a minimum difference of 3% was observed in beams 4Cont-M8-2 and 7Cont-M3-2.5.
- The shear span-to-depth ratio showed a negligible effect in predicting the effective moment of inertia for beams having the same steel reinforcement ratio and sectional properties.
- Both analytical and experimental results showed relatively good agreement in terms of the ultimate load and maximum displacement for all beams.
- Branson’s analytical equation presented either higher or lower stiffness before and after the cracking moments. Which shows some discrepancy using the equation in predicting the load-deflection history of HSC beams reinforced with no stirrups.

- For HSC beams reinforced with same size and number of stirrups, and tested under variable shear span-to-depth ratio, Branson's equation over- predicted the deflection due to the lower stiffness behavior.
- When the applied moment exceeds the cracking moment a sudden drop in the effective moment of inertia was observed. Beams with lower shear reinforcements showed a higher decrease in the effective moment of inertia compared to beams with the heavier shear reinforcement.
- Branson's analytical model showed more overall stiffness behavior before and after the cracking moment for beam 2CONT-MN-2.0 however that was not the case for 3CONT-MN-2.5, where the Branson's equation underestimated the displacement at the same load level.
- Beams with same shear reinforcement (#3@8 in.), and with (a/d) = 2.5 showed the highest decrease in the effective moment of inertia while the beam with (a/d) =3.0 showed the lowest decrease in effective moment of inertia.
- The deflection of HSC beams reinforced with carbon and glass fiber grids, predicted by four different empirical equations was underestimated at the ultimate stage by 38%, and 26%, respectively.

References

1. American Concrete Institute (ACI). (2016). ‘‘Building code requirements for structural concrete and commentary.’’ ACI 318-95, Farmington Hills, Mich.
2. ASTM C39, “ASTM C39 Standard Test Method for Compressive Strength of Cylindrical Concrete Specimens,” in ASTM Standard Book, 2016, pp. 1–5.
3. ASTM C496/C496M, “Standard Test Method for Splitting Tensile Strength of Cylindrical Concrete Specimens,” Am. Soc. Test. Mater., pp. 1–5, 2011.
4. ASTM C78 / C78M-16, Standard Test Method for Flexural Strength of Concrete (Using Simple Beam with Third-Point Loading), ASTM International, West Conshohocken, PA, 2016, www.astm.org.
5. ACI Committee 440, Guide for the Design and Construction of Structural Concrete Reinforced with FRP Bars, American Concrete Institute, Farmington Hills (MI), 2015.
6. ACI Committee 440, Guide for the Design and Construction of Structural Concrete Reinforced with FRP Bars, American Concrete Institute, Farmington Hills (MI), 2006.
7. Bank, C. L., Yehoshua, F., and Shapira, A. (1997). ‘‘Three-dimensional fiber-reinforced plastic grating cages for concrete beams: A pilot study.’’ ACI Struct. J., 94(6), 643–652.
8. Banthia, N., Al-Asaly, M., and Ma, S. (1995). ‘‘Behavior of concrete slabs reinforced with fiber-reinforced plastic grid.’’ J. Mat. in Civ. Engrg., ASCE, 7(4), 252–257.
9. Benmokrane, B., Chaallal, O., and Masmoudi, R. (1996). ‘‘Flexural response of concrete beams reinforced with FRP reinforcing bars.’’ ACI Struct. J., 91(2), 46–55.
10. Benmokrane, B., Masmoudi, R., Chekired, M., Rahman, H., Debbache, Z., and Tadros, G. (1999). ‘‘Design, construction, and monitoring of fiber reinforced polymer reinforced concrete bridge deck.’’ Proc., 4th Int. Symp. Fiber Reinforced Polymer Reinforcement for Reinforced Concrete Struct., American Concrete Institute, Detroit, 87–102. ‘‘Glass fiber reinforced polymer rebar.’’ (1997). Product Brochure, Hughes Brothers, Inc., Seward, Nebr.
11. Brown, L. V., and Bartholomew, L. C. (1993). ‘‘FRP reinforcing bars in reinforced concrete members.’’ ACI Mat. J., 90(1), 34–39.

12. C. Barris, L. I. Torres, A. Turon, M. Baena, and A. Catalan, “An experimental study of the exural behaviour of GFRP RC beams and comparison with prediction models,” *Composite Structures*, vol. 91, no. 3, pp. 286–295, 2009.
13. Engel RS, Bakis CE, Nanni A, Croyle M. FRP grid performance in concrete beams: an investigation of preform architecture. Int Conf Compos Infrastructure 1998:2.
14. Engel RS, Croyle MG, Bakis CE, Nanni A. Deflection of reinforced concrete beams reinforced by fiber reinforced polymer grids with various joint designs. 4th int symposium fiber reinf polym reinf reinf concr struct (FRPRCS-4), SP- 188, American Concrete Institute, Farmington Hills, MI 1999:75-85.
15. Fang, H., Zou, F., Liu, W., Wu, C., Bai, Y. and Hui, D. (2017).” Mechanical performance of concrete pavement reinforced by CFRP grids for bridge deck applications. Composites Part B 110, PP.315-335.
16. Goldston, M.W., Remennikov, A., Neaz Sheikh, M. (2017). “Flexural behavior of GFRP Reinforced High Strength and Ultra-High Strength Concrete Beams”, Construction and Building Materials 131, pp.606–617.
17. Goodspeed, C., Schmeckpeper, E., Yost, J. R., and Gross, T. (1990). ‘‘Fiber reinforced plastic grids for the structural reinforcement of concrete.’’ Proc., 1st Mat. Engrg. Congr., ASCE, New York, 593–604.
18. M. Noe and K. Soudki, “Estimation of the crack width and deformation of FRP-reinforced concrete exural members with and without transverse shear reinforcement,” *Engineering Struc- tures*, vol. 59, pp. 393–398, 2014.
19. Masmoudi, R., Theriault, M., and Benmokrane, B. (1998). ‘‘Flexural behavior of concrete beams reinforced with deformed fiber reinforced plastic reinforcing rods.’’ ACI Struct. J., 95(6), 665–675.
20. Matta F, Galati N, Nanni A, Ringelstetter TE, Bank LC, Oliva MG. Pultruded grid and stay-in-place form panels for the rapid construction of bridge decks. Compos convention trade show, American Composites Manufacturers Association: Columbus, OH 2005:1-9.
21. Matthys S, Taerwe L. Concrete slabs reinforced with FRP grids. I: one-way bending. ASCE. J Compos Constr 2000;4(3):145e53.

22. Mustafa, S.A., and Hilal, A.H. (2017). "Behavior of concrete beams reinforced with hybrid steel and FRP composites. Housing and Building National Research Center, HBRC Journal (Article in Press).
23. NEFCOM Corporation. (1990). ''Mechanical properties of NEFMAC.'' Tokyo.
24. P. H. Bischo , "Reevaluation of de ection prediction for con- crete beams reinforced with steel and ber reinforced polymer bars," *Journal of Structural Engineering*, vol. 131, no. 5, pp. 752– 762, 2005
25. Rizkalla S, Lucier G, Dawood M. Innovative use of FRP for the precast concrete industry. Adv Struct Eng 2012;15(4):565e74.
26. Shao YT, Mirmiran A. Control of plastic shrinkage cracking of concrete with carbon fiber-reinforced polymer grids. J Mater Civ Eng 2007;19(5):441-4.
27. Yang, W.R., He, X., Dai, L. (2017). "Damage behavior of concrete beams reinforced with GFRP bars. Composite Structures 161 (2017) 173–186.
28. Yost, J. R. and Schmeckpeper, E.R., (2001). "Flexural Behavior of Concete Beams Reinforced with FRP Grids". *Journal of Composites for Construction*, Vol. 5, No. 1, pp. 18-25.
29. Yost, J. R. and Schmeckpeper, E.R., (2001). "Strength and serviceability of FRP Grids Reinforced Bridge Decks". Journal of Bridge Engineering, Vol. 6, No. 6. pp. 605-612.
30. Zhang B, Masmoudi R, Benmokrane B. Behaviour of one-way concrete slabs reinforced with CFRP grid reinforcements. Constr Build Mater 2004;18(8): 625-35.
31. State-of-the-Art Report on High-Strength Concrete, ACI 363R-92, Farmington Hills (MI), 2015.
32. Sherif, A.G. and Dilger, WHO., "Critical Review of CSA A23.3-94 Deflection Prediction for Normal and High Strength Concrete Beams," Canadian Journal of Civil Engineering, Vol. 25, 1998, pp. 474-489
33. Al-Zaid, R.Z., Al-Shaikh, A.H., and Abu-Hussein, M.M., "Effect of Loading Type on the Effective Moment of Inertia of Reinforced Concrete Beams," ACI Structural Journal, Vol. 88, No. 2, March-April 1991, pp. 184-190.

34. Rangan, B.V., “Control of Beam Deflections by Allowable Span-Depth Ratios,” ACI Journal, Vol. 79, No. 5, Sept. Oct. 1982, pp. 372-377.
35. Alsayed, S.H., “Flexural Deflection of Reinforced Fibrous Concrete Beams,” ACI Structural Journal, Vol. 90, No. 1, Jan.-Feb. 1993, pp. 72-76.
36. Lotfy, B.M.S., “Deflections of R.C. Beams with Different Reinforcement Ratios,” CERM, Vol. 17, No. 3, March 1995, pp. 1062-1074.